Mechano-Pneumatic Wheel: Feasibility Analysis of the Concept and Parametric Optimization

Aswathy Mariyam Thomas

A Thesis

in

The Department of

Mechanical, Industrial and Aerospace Engineering

Presented in Partial Fulfillment of the Requirements for the Degree of

Master of Applied Science (Mechanical Engineering) at Concordia University

Montreal, Quebec, Canada

December 2024

Concordia University Concordia University

School of Graduate Studies

This is to certify that the thesis prepared

By: **Aswathy Mariyam Thomas**

Entitled: **Mechano-Pneumatic Wheel: Feasibility Analysis of the Concept and Parametric Optimization**

and submitted in partial fulfillment of the requirements for the degree of

Master of Applied Science (Mechanical Engineering)

complies with the regulations of this University and meets the accepted standards with respect to originality and quality.

Signed by the Final Examining Committee:

____ Chair

Dr. Hamid Taghavifar

____ Examiner

Dr. Waizuddin Ahmed

____ Supervisor

Dr. Subhash Rakheja

____ Supervisor

Dr. Ramin Sedaghati

Approved by ____

Dr. Muthukumaran Packirispamy, Chair,

Department of Mechanical, Industrial and Aerospace Engineering

13th January 2025 ____

Dr. Mourad Debbabi, Dean

Gina Cody School of Engineering and Computer Science

Abstract

Mechano-Pneumatic Wheel: Feasibility Analysis of the Concept and Parametric Optimization

Aswathy Mariyam Thomas

This research thesis presents the development and analysis of a novel Mechano-Pneumatic Wheel (MPW) by integrating the strengths of both pneumatic and non-pneumatic wheels. While pneumatic tires provide excellent comfort and traction, they are prone to punctures and require frequent maintenance. In contrast, non-pneumatic tires are durable and require low maintenance but often fall short in ride quality and versatility. The proposed MPW concept bridges this gap by integrating air springs arranged radially within a structural shear band. This study explores several MPW configurations, focusing on different air spring coupling methods, to optimize load sharing and road contact pressure distribution. A quasi-static model was subsequently developed to predict the wheel's deflection and load-bearing behaviour and validated using Finite Element Analysis and MATLAB simulations. A parametric investigation was conducted to study the influences of important design variables such as air spring size, configuration, and charge pressure on vertical stiffness. Optimization techniques, including genetic algorithms were applied to identify the optimal design parameters, achieving a target vertical stiffness of 190 kN/m while minimizing fluctuations in load distribution. The research study also incorporates a composite shear band which is modeled as a curved Timoshenko beam to improve its performance. A 3 mm reduction in the wheel's contact patch deflection was achieved with the addition of the shear band. By combining the best features of pneumatic and non-pneumatic wheel technologies, the present research introduces a versatile and innovative wheel concept with promising applications in automotive, aerospace, and off-road mobility.

Acknowledgements

I would like to extend my deepest gratitude to all those who have supported me throughout the course of my research and dissertation. Without their help, this work would not have been possible.

First and foremost, I would like to express my deepest gratitude to my supervisors, Dr. Subhash Rakheja and Dr. Ramin Sedaghati, for their invaluable guidance, encouragement, and expertise throughout the course of this research. Their unwavering patience, support and constructive feedback have been indispensable in shaping the direction and outcome of this work. I am truly grateful for their mentorship and for challenging me to expand my thinking, which has been instrumental in the success of this dissertation.

I am eternally grateful to my dad K. G. Jolly and mom Seba Mathew, for their unconditional love, support, and sacrifices, which have provided the foundation for all my achievements. I am also grateful to my aunt Santhi Thomas and uncle Sajan Thomas, my brother Sidharth Thomas and all my family who supported and helped me through the difficult periods. Their unwavering belief in me has been my source of strength and inspiration.

I would also like to acknowledge my colleagues, specifically Abolfazl Seifi, for his support and mentorship and for the many insightful discussions, shared knowledge and good times that made this journey memorable.

I would like to specifically thank my dear friends Vijesh, Nitheesh, Sophie and Judy for their support, encouragement and belief in me even during the most difficult and trying times. This work would not have been possible without their countless selfless acts of love and kindness.

Table of Contents

List of Figures

List of Tables

Nomenclature

E	Young's Modulus
G	Shear Modulus
CAD	Computer-Aided Design
FEA	Finite Element Analysis
NPW	Non-Pneumatic Wheel
NPT	Non-Pneumatic Tire
ME	Mechano-Elastic
MPW	Mechano-Pneumatic Wheel
θ	Half Contact Patch Arc angle
φ	Angular position of a tire element in the contact patch from the wheel's vertical axis
R	Unloaded radius of the wheel
R^*	Loaded radius of the wheel
$\boldsymbol{r_0}$	Rim radius of wheel
x	Horizontal component of the position vector
$f(x,\varphi)$	Radial displacement function of a tire element in the contact patch
k_s	Axial static stiffness of an air spring
k_{s1}	Axial deflection component of the stiffness of the air spring
k_{s2}	Effective area change component of the stiffness of the air spring
P_o	Absolute pressure inside the air spring
P_g	The gauge pressure inside the air spring
P_{at}	Atmospheric pressure
F_a	Elastic force developed in the air spring

A_e	Effective area of the air spring
N	Polytropic gas index
V	Volume of the air spring
F_z	Applied vertical load
F_v	Resultant vertical elastic force of all the air springs
P_1	The increased pressure inside the wheel after the application of F_z
A_o	The constant nominal area of air springs
$W_{in,M}$	Mechanical work done on the wheel as it is loaded
Δz_i	The deflection of the i^{th} air spring in the contact patch under F_z
Δz	The deflection of air springs outside the contact patch
U	The internal energy of the air inside the wheel
dV_i	Change in volume of the i^{th}air spring
n_{cp}	The number of air springs undergoing deflection in the contact patch
K_z	The equivalent vertical stiffness of the MPW without Tread stiffness
K_{eq}	The equivalent vertical stiffness of the MPW with Tread stiffness
F_{tz}	The net vertical components of the spring forces
δ_{ti}	Deflection of i^{th} spring element in the tread
$g(x, \varphi)$	Radial displacement function of a a tread element
K_t	The effective stiffness of the tread
D	Diameter of an air bag
h_0	Nominal design height of the air bag
V_0	Volume of the reservoir
n	Number of air bags

u_r	Radial displacement
u_θ	Circumferential displacement
Φ	Rotation of the beam cross-section
EA	Axial Stiffness
EI	Bending Stiffness
GA	Shear Stiffness
$u_r(\theta)$	The transverse displacement
$u_\theta(\theta)$	The circumferential displacement
$\phi(\theta)$	The cross-section rotation with respect to the centroid of the cross-section
Z	The thickness variable
ε_{rr}	Radial strain
$\varepsilon_{\theta\theta}$	Circumferential strain
$\gamma_{r\theta}$	Shear strain
M	Bending moment
N	Axial force
V	Shear force
$\sigma_{\theta\theta}$	Tangential stress
$\tau_{r\theta}$	Shear stress
δV	External virtual potential energy

Mechano-Pneumatic Wheel: Feasibility Analysis of the Concept and Parametric Optimization

Chapter 1. Introduction and Literature Review

1.1 Introduction and Background

The effectiveness of ground vehicle dynamics heavily relies on the interactions between the tires and the ground. Conventional pneumatic tire designs have long been the foundation of vehicular mobility, having several key attributes such as effective force transmission, ride quality, road holding, handling etc. However, the recent efforts to overcome challenges to eliminate tire pressure loss, higher maintenance requirements, and environmental hazards have brought a need for innovative wheel solutions. This chapter provides the background, motivation, and review of recent relevant studies to build the scope of the thesis and to gain essential knowledge and method of analysis.

Pneumatic tires are an indispensable component of modern ground vehicles. These serve the primary functions of providing the interface between the vehicle and the terrain, supporting the vehicle load, and providing friction to transfer tractive forces to the ground for acceleration, braking, and cornering of the vehicle. Pneumatic tires also act as a spring and damper system for absorbing terrain-induced vibrations. Although seemingly simple to the oblivious consumer, modern pneumatic tires are highly engineered structural composites whose performance can be designed to meet the vehicle manufacturer's ride, handling, and traction criteria, as well as the quality and performance expectations of the consumer [1].

The first known wheels were solid wooden discs and were used for pottery, in wheelbarrows, carts, and chariots in the ancient civilizations of Mesopotamia, China, and Europe as early as 4000

BC. These wheels were primitive and could only withstand a limited amount of wear and tear. They were heavy and did not have any ground-induced vibration-absorbing properties, thereby producing bumpy rides. Eventually, spoked wheels which consisted of a hub with radiating spokes, connected to a rim, emerged. This design reduced the weight of the wheel while maintaining its structural integrity. Subsequently, wheels with iron rims were developed to reinforce the wood. By the mid-19th century, leather strips and rubber bands began to be fitted to wheel rims to soften the ride of early wagons, coaches, and carriages.

In 1844, Charles Goodyear discovered the process of Vulcanization of Rubber, which enabled rubber to be made durable to the elements while preserving its elasticity. Following this, the first air-filled vulcanized rubber tire was invented in 1845 by Scottish Inventor Robert William Thomson. It was called an 'Aerial Wheel', and it used a rubberized fabric tube filled with pressurized air and encased in a thick leather outer skin and was bolted to the rim. Although the Aerial wheel yielded improved ride comfort and durability compared to the conventional spoked solid wheel, and though British, French, and US patents were granted for the design, the cost of construction of the pneumatic bladder was too high to make the invention accessible for general use. Thomson's Aerial Wheel was invented with the aim of improving the ride quality of carriages. Bicycles were uncommon at the time of his invention of the Aerial Wheel and eventually, it was forgotten. In 1888 a Scottish inventor and Veterinarian, John Boyd Dunlop created an air-filled rubber tire for improving the riding comfort of his son's bicycle. Owing to the booming popularity of bicycles and the cheaper cost of manufacturing his air-filled tires at the time, his invention grew in popularity and soon began to be mass manufactured for bicycles. Seven years after Dunlop's invention, in 1895, the Michelin brothers, Andre and Edouard used pneumatic tires for the first time in an automobile in the Paris-Bordeaux race. However, they were not durable. It wasn't until the invention of the combination of tire and inner tube by Philip Strauss in 1911 that pneumatic tires began to be widely accepted and used in automobiles following which, the tire industry grew rapidly. Some of the milestones in its growth were the development of synthetic rubber by DuPont in 1931, and the development of the radial-ply tire by Michelin in 1948. Over the last century, pneumatic tires have become a vital component of ground vehicles due to their many merits such as low energy dissipation on rough grounds, decreased vertical stiffness, reduced contact pressure, and low mass [2] resulting in a relatively high natural frequency of the un-sprung mass, thereby providing an improved ride quality.

1.2 Literature Review

The study of automotive wheel encompasses many challenges associated with structure, design, vehicle performance, environmental concerns, manufacturability and sustainability. Relevant reported studies in all these subject areas are systematically reviewed and summarised below under appropriate groups. Furthermore, it identifies shortcomings in existing tire technology and emphasizes the need for a new wheel design.

1.3 Developments in Pneumatic Tires

Pneumatic tires have undergone significant advancements, driven by the need to optimize their performance across various applications. Research has focused not only on improving tire efficiency and durability but also on understanding the fundamental interactions between tires, materials, and surfaces. These efforts have paved the way for innovations in tire design and modeling, addressing both practical challenges and performance demands.

Darrow [3] presented an extensive overview of the historical and technical advancements in pneumatic tires, tracing their evolution from the mid-19th century to the early 20th century. Beginning with Robert William Thomson's 1845 patent, the study highlights Thomson's innovative understanding of pneumatic principles, such as the use of layered structure, cushioning properties, and reduced noise during motion. Although Thomson's design laid the groundwork, it was John Boyd Dunlop's 1888 patent that marked the true beginning of the pneumatic tire industry. Dunlop's contributions, particularly the development of inflatable tires for bicycles and later motor vehicles, established a foundation for continuous innovation in tire technology. One key advancement in the development of Pneumatic tires is the transition from fabric-based tire construction to rubber cord materials [3]. Early tires primarily used heavy woven fabrics, which were eventually replaced by high modulus cords 1914. Cords offered superior flexibility, reduced power consumption, and enhanced durability, addressing many of the limitations of fabric layer tires. Despite initial challenges, such as rim and bead failures, cord-based tires quickly became the standard for passenger and commercial vehicles. The paper also examined the evolutions in tire design to accommodate growing demands for performance and versatility. The introduction of balloon tires in the 1920s represented a significant shift toward lower inflation pressures and wider cross-sections, which improved ride comfort, traction, and load distribution. These designs culminated in the development of super-balloon tires, which further reduced pressure requirements and enhanced stability, especially for heavy vehicles and industrial machinery [3].

Darrow [3] further highlighted the emergence of specialized tires tailored for distinct applications. For example, pneumatic lug tires were developed for agricultural and road-building equipment, offering better traction on soft or uneven surfaces. Similarly, air wheel tires were designed for aircrafts, providing shock absorption and stability during landing, while rail-car pneumatic tires demonstrated the adaptability of this technology across guided transportation modes. Operational challenges, such as heat generation, track conditions, and overloading, were also key considerations in tire development. Darrow [3] emphasized the role of compounding materials and design adjustments in mitigating heat-related damage and extending tire life. Moreover, advancements in rubber technology, tire testing and manufacturing techniques were crucial in achieving consistency and reliability in modern tire designs.

Tarasov et al. [4] employed the method of sections and utilized secant planes and cylindrical surfaces to derive equilibrium equations for critical tire components, including the equator and bead rings. This method introduced new computational schemes that improved the precision of forces and tire capacity estimations, enabling more effective structural optimization. Additionally, their work highlighted the influence of tire contact area on rolling resistance and wear, offering valuable insights into tire performance and durability [4].

Freitag [5] presented valuable insights into the interactions between pneumatic tires and soft soils. Using dimensional analysis, the study identified key parameters such as pull, sinkage, and torque that describe tire performance. Experiments with pneumatic tires of varying sizes were then conducted on wet, frictionless clay and dry, cohesionless sand under controlled conditions. Notable findings include the use of cone penetrometer measurements to assess soil strength and the potential for true scaling between model and full-scale systems. The study also introduced consolidated terms for clay and sand, linking soil and tire parameters to performance, while highlighting challenges in consistency and scaling [5].

Popescu et al. [6] noted the need for a centralized system for inflation pressure for agricultural tractor tires and conducted experimental investigation of an inflation system. Edeskär [7] utilized the geometric characteristics and consecutive equations of materials comprising pneumatic tire and rim to establish tire pressure relation. The method used physical properties of material such as elasticity and deformation and material data of tire to estimate tires' pressure-deflection relation. Roth et al. [8] considered a 2D model and rigid surface to estimate a correlation between tire characteristics and contact patch area, which is the area of a tire in contact with a rigid surface in a 2D environment. Kenarsari et al. [9] developed the 3D model of the wheel to further study the interaction between the tire and the contact patch by carrying out a dynamic analysis of the tire model. Apart from these studies which focused on traditional tire configurations, technological improvements of tires introduced Improved Flexion (IF) and Very High Flexion (VHF) tires, enhancing tire tread profiles to improve performance. Melzi et al. [10] also considered elastic, mechanical, and geometrical properties of tires considering the tire as a damper-spring system.

1.3.1 Limitations of Pneumatic Tires

Pneumatic tires have evolved over time offering comfort, longevity and durability, demonstrating versatility in various conditions [2], but despite their proven performance and advantages over their predecessors, these exhibit many inherent drawbacks. Although currently, these deficiencies are milder than in the early designs of pneumatic tires, these exist and are prominent enough to motivate further developments to eliminate their inherent disadvantages and investments into exploring non-pneumatic wheels which combine the advantages of pneumatic tires without their characteristic complications and limitations [2].

Some of the major deficiencies of conventional Pneumatic tires are that they are vulnerable to damage, particularly on rough terrains, sharp objects, and potholes. Over time, these damages can lead to tire wear, sidewall damage, or even structural failure and resulting in loss of vehicle performance and control in the event of a tire bursting [11,12]. High-speed impacts or running over curbs can cause sidewall bulges or blowouts, which pose safety risks. It has been reported that 70% of total accidents on highways stem from tire blowouts, which often lead to body injuries and fatalities especially when the failures occur at relatively high speeds [13]. Pneumatic tires require regular maintenance of proper tire pressure. Changes in temperature and use can lead to fluctuations in tire pressure, requiring regular checks and adjustments. Insufficient tire pressure can negatively impact handling, fuel efficiency, heat generation and overall tire performance. Repairing or replacing a damaged or worn-out Pneumatic tire can be costly, especially for larger vehicles or specialized equipment that require specific tire sizes. The manufacturing process for Pneumatic tires is also complex. The disposal of used Pneumatic tires has significant environmental and human health impacts [14–17]. The mechanics of the pneumatic tire places limitation of the range of flexibility for its design. The stiffness along its three axes is strongly coupled making it impossible to vary one for improving a particular performance parameter without compromising another [2]. These shortcomings associated with pneumatic tires have led to the emergence of non-pneumatic wheel models. NPWs offer promising solutions to many of the limitations associated with conventional pneumatic tires, especially in view of pressure failures.

1.3.2 Non-Pneumatic Tires

A number of studies investigated feasible non-pneumatic alternatives to conventional pneumatic tires since the 1900s. A non-pneumatic tire typically consists of three components: the tread, rim, and the support structure. Non-pneumatic tires have a simpler construction than conventional pneumatic tires. This straightforward construction enables non-pneumatic tires to achieve an independent, reduced coupling between vertical, lateral and longitudinal stiffness, and ground pressure while overcoming the coupling limitations of several mechanical attributes of conventional pneumatic tires [18–20]. In the place of air in a conventional pneumatic tire, NPWs employ either flexible radial spokes [21–23] or honeycomb lattice spokes [24–26]. Because the load-bearing element of non-pneumatic tires (NPTs) is not air, they do not have the safety issues associated with punctures and air leakage as in Pneumatic tires. NPTs also have a wider degree of freedom in their design, hence they have a higher range of load-carrying capacity than their pneumatic counterparts [19,20,27].

Studies have shown that NPWs can have the same merits associated with pneumatic tires without the risk of a flat tire or routine maintenance. NPWs have the advantage of superior tunability compared to pneumatic tires. The vehicle handling and cornering can also be improved by tuning the lateral stiffness without compromising the ride quality, which is determined by the vertical stiffness [19,20,27]. Moreover, because of the reduced maintenance requirements of NPWs, they are expected to be more sustainable and environmentally friendly compared to the pneumatic tires [19,20,27].

The choice of materials for non-pneumatic tires is likewise more open. Options for non-pneumatic tire materials include polymer materials with high strength and superior cushioning capabilities as well as environmentally friendly recyclable materials [19,27]. These options are all significant alternatives to conventional rubber materials and associated additives.

One of the primary requirements for an NPWs' design is that their supporting structures must exhibit both flexibility and resilience, like how the compressed air in a pneumatic tire undergoes cyclic tension and compression to provide these properties [13,16,28]. These are two conflicting features in any material. However, in NPWs, the geometry and material properties of the spokes are utilized to invoke both these qualities to replicate the behavior of air in a pneumatic tire [16]. A comprehensive review of the existing literature on the studies that have been conducted to model and understand the various static and dynamic performance parameters of different types of NPWs is presented below. The review starts with the radial spoked Tweel™ and follows with NPWs with honeycomb spokes and subsequently, the Mechano-Elastic wheel.

1.3.2.1 Radial Spoked Tweel^{TM}

Over the years, various conceptual designs of NPWs have emerged. Figure 1-1 shows the integrated tire wheel unit consisting of flexible radial spokes connecting a circular elastic shear beam to the hub, which was first proposed by Rhyne and Cron [2]. Following this, there have been extensive studies on developing analytical and numerical models for this design and eventually Michelin developed the Tweel^{TM} which features curved radial spokes as shown in Figure 1-2 [29]. Several studies are continuing to investigate properties of the Tweel^{TM} [30,31]. Although the tweel has been purported to have superior ride and handling, low mass, lower contact pressure, and lower energy losses compared to other models of NPWs, studies have reported unacceptably high noise and vibration of the spokes under high-speed rolling conditions which resulted in poor ride comfort [30]. It was found that induced noise was likely associated with the self-excited resonant vibration of the spokes of the Tweel^{TM} due to their cyclic buckling and snap back to tension as they enter and leave the contact zone. Numerical and experimental studies on the effect of spoke geometry such as spoke length, spoke thickness, spoke curvature, and shear band material characteristics and thickness on the vibration levels have been conducted [32]. Among the spoke geometry parameters, spoke length was found to have the most significant impact on the amplitude of the vibration. The effect of the same geometrical parameters on the contact pressure, vertical stiffness and rolling resistance of the Tweel^{TM} have also been investigated in a few studies [30–32].

Further parametric analysis and sensitivity studies have shown that the shear modulus of the material of the shear band, Polyurethane, and the thickness of the shear band are the most important parameters that determine the tire performance measures. A higher shear modulus of the polyurethane and higher shear band thickness has been proven to produce low rolling resistance [33,34]. Rugsaj and Suvanjumrat [35] modified the existing analytical model of the NPW which considered only the shear deformation of the shear beam, to incorporate both bending and circumferential extension based on the curved beam theory. The model was developed considering a two-dimensional quasi-static theory. The model was able to predict the spoke thickness which gives the same vertical stiffness as an equivalent pneumatic tire which was verified using FE analysis.

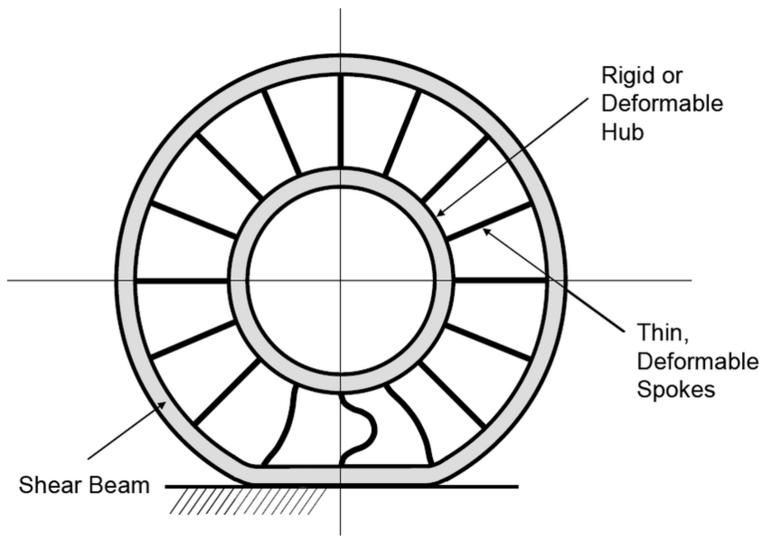

Figure 1-1 Deformation of the generic Tweel™ proposed by Rhyne et al. [2]

Figure 1-2 Michelin's Tweel™ [29]

1.3.2.2 Honeycomb Wheel

Another promising NPW is the honeycomb structured spoke design. The spokes in this design are made of a lattice of hexagonal, square, diamond, or other honeycombs as shown in Figure 1-3 [36]. Recent studies have shown that honeycomb structures in NPWs give several desirable properties comparable to those of the pneumatic tires and they have high flexibility with greater design owing to the dependence of their properties on the cell geometry [16,24].

Figure 1-3 Honeycomb NPW launched by Polaris Industries Inc. [36]

The Honeycomb NPW has been widely investigated in recent years using extensive analytical and numerical methods to study, the effect of types of cells and their geometry on the performance of an NPW. A comparative study of three types of NPWs with a pneumatic tire showed that the former has a much higher load-carrying capacity while having much lower peak stress in spokes and tread compared to a pneumatic tire [24]. NPWs with honeycomb spokes showed high value of initial vertical stiffness which decreased as load increased [16,24]. This is associated with cell wall's resistance to compression, which tends to decrease with cell buckling. Ju et al. [16] studied the effect of the geometry of the honeycomb on the load carrying capacity under uniaxial loading conditions. The flexibility of the honeycomb spoke was found to be primarily decided by the ratio of the inclined cell length and overall cell height. Although a lower cell expanding angle was found to be favorable for a higher load carrying capacity, spokes with a higher cell expanding angle demonstrated better fatigue resistance owing to lower local stresses. [16,24]Kim et al. [25] also studied the effect of vertical load on static contact pressure in NPWs with hexagonal honeycomb spokes and found that since the vertical stiffness of the NPW decreases with vertical load, and due to the high lateral stiffness of the spokes, NPWs in general show lower contact pressure compared to their pneumatic counterparts. Ju et al. [16] also established that contact pressure was affected by the cell angle. For NPWs with honeycomb spokes of auxetic nature [37,38], which have a negative Poisson's ratio, a higher negative cell angle resulted in lower pressure distribution along the contact patch. It was also found that comparing regular and auxetic hexagonal honeycombs, for the same load carrying capacity, the former had relatively lower local stress and mass. The NPW design with auxetic honeycomb spokes would thus result in a heavier structure than the one with the regular honeycomb spokes for the same load carrying capacity [24].

The dynamic properties of NPWs with honeycomb spokes with three different cell geometries but having the same cell wall thickness or load carrying capacity was studied by Jin et al [24]. It was found that the maximum stresses in the spokes and tread and the deformation in the spokes were much higher in dynamic loading than in the static loading. For NPWs designed with the same reference load carrying capacity, a lower cell expanding angle design had the highest load carrying capacity and the lowest mass. A lower cell expanding angle was also found to be preferred owing to lower rolling resistance by virtue of its lowest mass and least spoke deformation. The study concluded that a low cell expanding angle was ideal for a good load carrying capacity and low rolling resistance. Numerical studies on the modal behaviour and steady state vibration characteristics of NPWs with flexible regular and auxetic hexagonal honeycomb spokes for varying vertical loads and rolling speeds showed that the cell geometry of the honeycomb spokes is a key factor that affects the modal behaviour [37,38]. It has been observed that owing to the discrete geometry, orthotropic properties and non-homogenous mass distribution of the honeycomb spokes, there are local vibration effects unlike in a conventional pneumatic tire [38,39]

There has been extensive research on the development of analytical models for pneumatic tires. However, the problem of ground contact has generally been accounted by computational numerical methods. For the case of NPWs, a detailed analytical study of the contact region was first conducted by Rhyne and Cron [2]. The NPW was modeled as a thin flexible annular band that connected to the hub through the flexible spokes. The Euler-Bernoulli curved beam theory was used to model the wheel considering the major deformation modes as bending and shearing. Gasmi et al. [39,40] incorporated the extension of the shear band to the deformation modes and developed a quasi-static model of the NPW and was able to determine the pressure profile, vertical stiffness and rolling resistance during low-speed conditions.

1.3.2.3 Mechano-Elastic Wheel

Another NPW model with radial spokes is the Mechano-elastic (ME) wheel with the hinge-unit spoke design was proposed by Zhao et al [41]. Like the tweel, the ME-Wheel is an integrated tire and wheel assembly. The general model is shown in Figure 1-4 [42] which consists of the wheel hub, the hinge units, and the elastic outer wheel. In a ME wheel, both the flexible tire body and the bending deformation of the hinge units absorb the shock form road roughness [43].

There has also been research on mechano-elastic (ME) models of NPWs. Zhao et al. [41] investigated the multi axis stiffness of ME wheels with varying number of hinge structures through analysis of a numerical FE model which was verified with experimental results. The vertical stiffness of the ME wheel was found to increase with an increase in the number of hinge structure units [42]. Studies on the effect of tire geometry and shear band material properties on lateral stiffness of ME wheels showed that lateral stiffness of ME wheels decreased with an increase in the tire depth to width ratio, whereas it increased with an increase in the vertical load and shear modulus of the shear band [41,44].

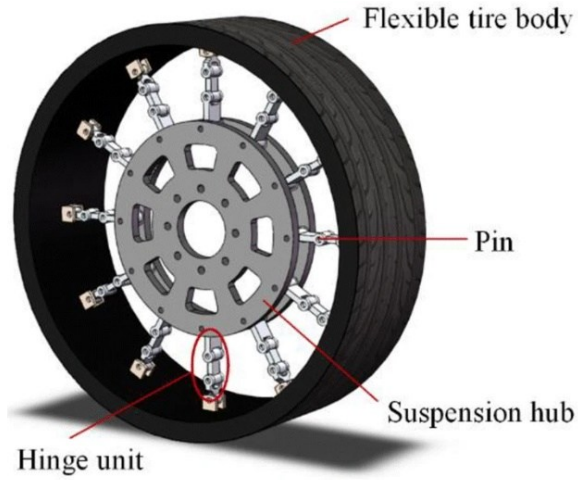

Figure 1-4 Schematic of the Mechano-Elastic wheel [42]

Du et al. [44] conducted a comparative study of the effect of camber angle on the grounding characteristics of a ME wheel with a pneumatic wheel. The results showed that although both the ME wheel and the pneumatic wheel suffered partial wear of the tread with an increasing camber angle, the pressure concentration of the ME wheel was much lower than its counterpart. A numerical FE study on the performance of the ME wheel with varying camber angle under static and dynamic rolling conditions was also conducted by Du et al. [45]. It was reported that in the static condition, with an increasing camber angle, the shape of the contact patch gradually changed from rectangular to triangular and the contact pressure was mainly concentrated at the shoulder of the ME wheel, which would ultimately result in an uneven wear of the tire. Studies on the natural frequency of ME wheels have also shown the significance of several factors such as elastic modulus, loads, torques and structural factors. With an increase in their respected values, it was found that the natural vibration frequencies ME wheel were also increased. The ground constraints also affected the mode of vibration [46].

1.3.3 Relative Benefits of NPTs

NPWs offer enhanced durability, reliability, and performance across diverse operating conditions. By eliminating the need for pressurized air, NPWs eliminate the risk of tire bursts and rapid pressure loss, enhancing vehicle safety and reliability and hence making them ideal for applications involving continuous operations and minimal maintenance are critical. Additionally, the elimination of air pressure reduces the maintenance requirements and operation costs. NPWs also offer a wide range of architectural possibilities to adapt to the requirements such as increased surface area or variable stiffness requirements. Furthermore, NPWs often exhibit simpler manufacturing processes and reduced environmental impact compared to pneumatic tires, making them potentially more sustainable and cost-effective in the long term. Owing to these advantages over pneumatic tires, NPWs have the potential for application in a wide range of industries. Figure 1-5 [47–50] shows a few examples of various industries that have adapted NPWs over pneumatic tires.

Military vehicles use NPWs to eliminate punctures, bursts, or rapid air loss enabling operation in diverse and challenging terrains. NPWs offer improved puncture resistance, traction, and stability on uneven surfaces such as mud, gravel, and rocks for off-road vehicles. Within the agricultural industry, using NPWs provides a reduction of soil compaction, with enhanced traction, enabling farmers to operate in varying soil conditions and minimizing downtime. NPWs are also used in Unmanned Aerial Vehicles, lunar rovers, mining equipment, construction machinery, and medical mobility devices. The simplicity of NPW design creates opportunities for innovation, enabling specific solutions depending on the application requirements. As research and development efforts continue to advance NPT technology, the opportunities for their application and impact are expected to grow.

a) Autonomous agricultural machinery [47]

b) Resilient Technologies [48]

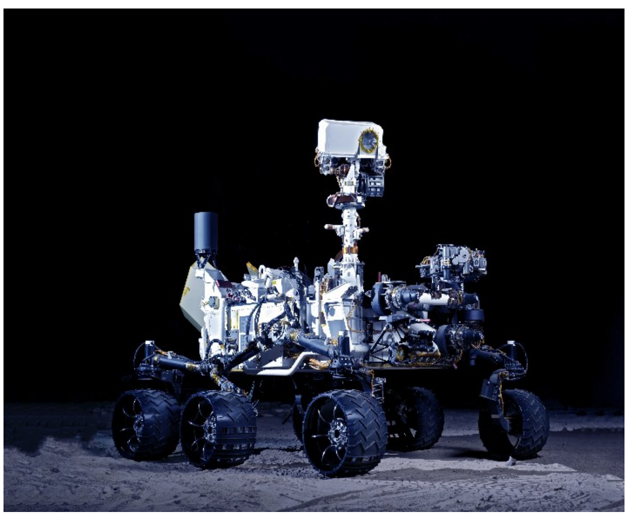

c) Curiosity rover NPT [49]

d) Polaris Sportsman WV850 [50]

Figure 1-5 NPWs in various industries [47–50]

1.3.4 Limitations to the Mainstream Utilization of NPWs

There have been considerable research efforts on the development of various models to study the static and dynamic characteristics of different kinds of NPWs, such as load carrying capacity, multi-axis stiffness along various axes, pressure distribution at the wheel-ground contact patch, stresses and deformations in the spokes and shear band, rolling resistance, and vibration response etc. For a comprehensive understanding on the applicability of the proposed NPW models, a relative performance study of the different NPWs and the equivalent pneumatic tire for the specific application has yet to be performed. This has been carried out in only a few studies [46,51]. Moreover, most of the studies were numerical in nature, and included developing a FE model using a commercial software, followed by its experimental verification [46,51]. Very few analytical models were reported in literature. Also, based on the reviewed studies, it can be inferred that load carrying elements (spokes) may experience permanent deformations under transient road loads, which would adversely affect vehicle performance and service life of the wheel. Relative deflection responses of airless wheels with different structures, namely, radial spokes, honeycomb, and triangular and diamond spoke patterns have shown that a diamond structure yields least deflection. A low-deflection wheel, however, will yield high stiffness and thus poor ride quality, and reduced contact area, which may adversely affect transfer of traction/braking forces. Apart from the flexibility along the fore-aft axis, a pneumatic tire offers considerable flexibility in the side-to-side direction to generate cornering force and self-aligning moment of the wheel, which is vital for good directional control and steering performance of the vehicle. The lateral force developed by the wheel is attributed to its side-slippage, which will cause lateral deformation of the honeycomb structure or the radial spokes. The lateral deformation behavior and the cornering property of the NPW have not yet been explored. Additionally, studies on NPW's ride handling capabilities and traction/braking are also limited.

1.3.5 Summary and Motivation: Need for an Innovative Wheel Concept.

The chapter reviews details on the evolution and advancements in non-pneumatic tire (NPW) technology. The review explores the design principles and engineering considerations underlying

NPWs, including structural configurations, materials selection, and performance characteristics. It discusses various NPW designs, such as radial flexible spokes, cellular honeycomb structures, and mechano-elastic systems, analyzing their strengths, limitations, and potential applications. The review also addresses the limitations of NPW models, such as ride comfort, handling, and manufacturing complexity. Most of the recent studies focuses on the non-pneumatic wheel counterparts which are not able to comprehend the advantages of pneumatic wheels. Noting the disadvantages of both pneumatic and non-pneumatic wheels, the focus should be on configurations which accumulates the advantages of both pneumatic and non-pneumatic configuration minimizing the disadvantages. The configurations which accumulate advantages of both pneumatic and non-pneumatic wheels called namely mechano-pneumatic wheels (MPWs) remain unexplored which is the major focus of current research thesis.

1.4 Thesis Objective and Scope

An alternate wheel design with flexible pneumatic spokes (air bags) may potentially provide the benefits in terms of the safety and puncture-resistance, and low maintenance as well as improved functional performance in terms of the ride comfort and handling. This study is aimed at the kineto-static analyses of a wheel design with pneumatic spokes. A design concept of the wheel with pneumatic struts, proposed by Autovector [52] as shown in Figure 1-6 [52] was initially explored. It was perceived that the struts may incur high stresses due to bending in the pitch and roll planes during acceleration/braking and cornering. Subsequently, an alternate design with inter-connected relatively flexible air spokes was conceived to minimize the bending stresses and to ensure maximum load sharing among the radial spokes via pneumatic couplings. An analytical model of the proposed design concept, denoted as 'Mechano-pneumatic wheel (MPW)', is formulated to study its kinematic behavior. A thermodynamic based formulation is presented to determine instantaneous air pressure within each radially positioned spoke, and the normal force distribution. The analyses are carried out for both independent (unconnected) and pneumatically coupled spokes. It is shown that the pneumatic coupling among the radial spokes enhances the load sharing among the spokes and thus yields more uniform load distribution compared to the uncoupled spokes. Parametric studies are subsequently performed to identify desirable design variables of the NPW considering the design objectives. These results are subsequently explored to identify the optimal design parameters, namely, the size and number of radial spokes.

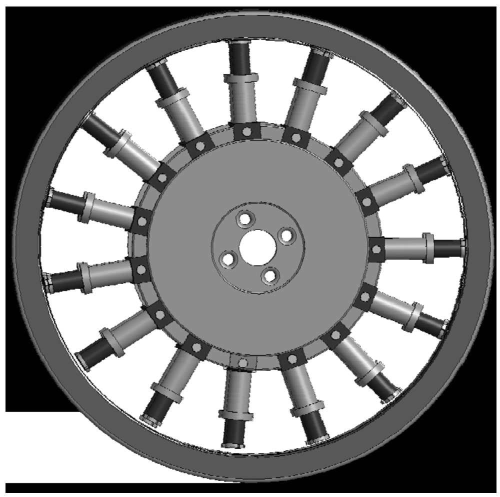

Figure 1-6 Conceptual Design of an Automotive Wheel with Pneumatic Struts Proposed by Autovector [52].

1.5 Organization of Thesis

The thesis is structured as follows. Chapter 1 provides details on the background and existing literature on Pneumatic tires and Non-Pneumatic Wheel (NPW) technology as well as motivation and objectives of the present research study. Chapter 2 address the novel design concept of the Mechano-Pneumatic Wheel together quasi-static analytical models and design optimization formulation. The modelling of the shear band is discussed in Chapter 3. Chapter 4 details a Finite Element Analysis on the developed Mechano-Pneumatic Wheel model to understand the effect of the shear band on the wheel model. Chapter 5 summarizes major conclusions and a brief description of the scope for future work.

Chapter 2. Design Concept, Modeling and Optimization of the Mechano-Pneumatic Wheel

2.1 Introduction

The conceptual Mechano-Pneumatic Wheel (MPW) utilizes pneumatic springs as the primary load-carrying element. The pneumatic springs are arranged radially around the rim in an integrated tire-wheel assembly. Figure 2-1 illustrates the proposed conceptual design of the MPW. Pneumatic springs are available as rigid piston-cylinder types or as air bag springs with flexible members made of rubber compounds. Owing to their flexibility, which would prevent the occurrence of high stresses in the pitch and the roll planes during acceleration, braking and cornering, air bags are the pneumatic spring of choice for the conceptual MPW [53,54]. The conceptual MPW design also consists of a sandwiched shear band and a rubber Tread, like other Non-Pneumatic Wheel designs.

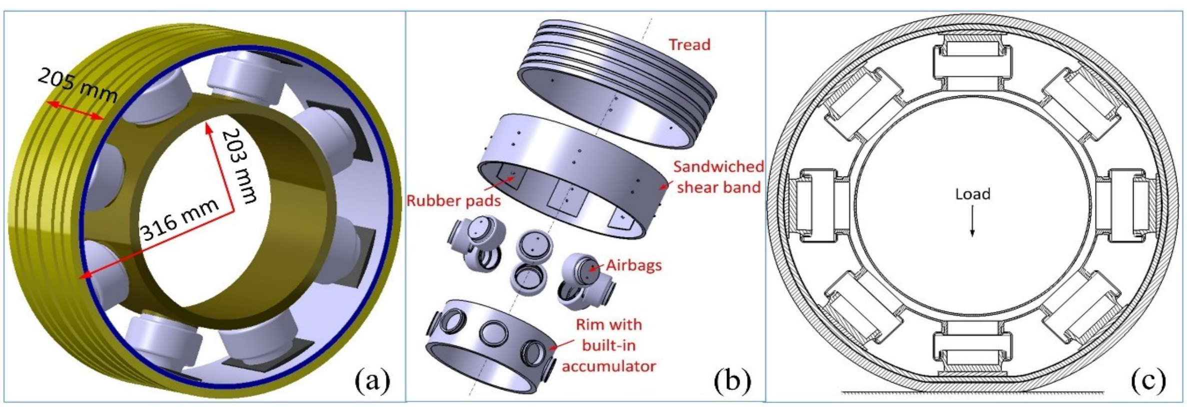

Figure 2-1 (a) conceptual design of a mechano-pneumatic wheel (MPW); (b) components of the MPW (c) sectional view of the MPW under load.

The proposed conceptual MPW design has several potential merits in comparison to the pneumatic tire. The conceptual MPW does not have a rubber compound carcass, and air springs with flexible members have a low hysteresis loss, it is thus expected to have a much lower internal friction and hence lower rolling resistance than a pneumatic tire. Since it is easy to achieve a variable spring rate and load-carrying capacity for air springs by tuning their charge pressure and internal volumes, the conceptual wheel design also presents the possibility of enhanced design flexibility as well as improved mobility performance on varying terrains through variations in the charge pressure and air volume. The conceptual design also presents a more sustainable wheel design, with reduced maintenance for wear and tear since it requires the replacement of the tread alone. Considering this, it also reduces the environmental hazards associated with the disposal of bulky tires made of rubber.

2.2 Design Configurations of the MPW

Depending on the connections between the air springs, three configurations of the MPW were conceived and studied. The first configuration consisted of stand-alone air springs, arranged radially around the rim of the wheel. In the second configuration, the radially arranged air springs around the wheel rim were connected through pneumatic connections between consecutive spokes to allow airflow among them in a serial manner. As seen in Figure 2-1(c) the third configuration consisted of a rigid toroidal reservoir, placed around the rim, to which all the radially positioned air springs were connected. The three design configurations are named the uncoupled, series-coupled, and parallel coupled configurations, respectively. In the parallel coupled MPW design configuration, the area of the orifice between each air spring and the reservoir is assumed to be identical to the cross-section area of the air spring. The pressure loss attributed to air flows between the air springs and the reservoir is thus neglected.

2.3 Quasi-Static Model of the MPW

The radially positioned air springs are the primary load-carrying members of the MPW. When the MPW, with its working volume charged to a reference pressure, is placed on the ground and is subjected to a vertical load, there is a vertical deflection and as a result, a contact patch is formed at the region of contact between the wheel and the ground. This vertical deflection corresponding to the applied vertical load, increases the internal energy of the air inside the working volume of the NPW. Correspondingly, the air spring elastic force generated by the air springs subjected to the increase in internal energy increases. It is this air spring elastic force that carries the vertical load in the conceptual MPW.

To study the feasibility of the conceptual MPW, a simple analytical wheel model that considers only the radial flexibility of the airbags based on the radial displacement of the wheel's circumferential elements is formulated[55]. In this preliminary model, the contribution of the tread is neglected, and the deformation of the shear band is limited to the segment in the contact patch. It is also assumed a non-rotating, loaded wheel, considering symmetric load distribution and deflection about the wheel's vertical axis, Figure 2-2 illustrates the radial displacements of the wheel's peripheral elements in the half-contact patch.

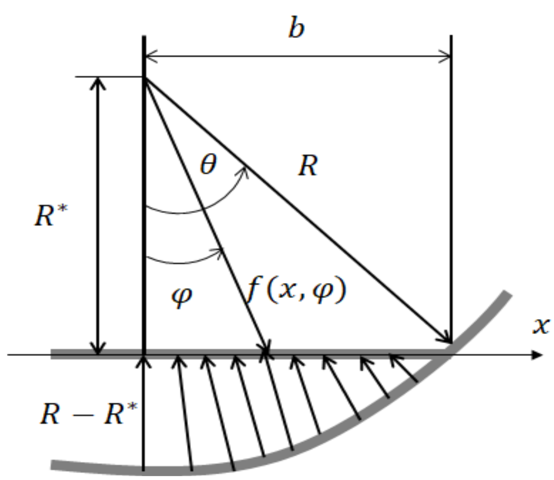

Figure 2-2 Geometrical representation of the displacement of a loaded wheel's peripheral elements in the half contact patch.

The half-contact patch is defined by the arc angle θ. Let R^* and R represent the loaded and unloaded radii of the wheel, respectively. Let x define the horizontal component of the position vector and φ denote the angular position of each peripheral element in the contact patch with respect to the wheel vertical axis.

The radial displacement of a peripheral element in the contact patch is defined by x and φ. From the geometry of the wheel, the radial displacement function of a wheel's peripheral elements in the contact patch can be expressed as,

$$f(x,\varphi) = R\frac{cos\theta}{cos\varphi} \quad \text{2-1}$$

The radial deflection of a peripheral element in the contact patch is given by,

$$R - f(x,\varphi) = R\left(1 - \frac{cos\theta}{cos\varphi}\right) \text{ where } -\theta < \varphi < \theta \quad \text{2-2}$$

For the MPW, the deflection given by Eq. (2-2) is the deflection of a radially positioned spoke in the contact patch.

2.4 Analytical Model of the Air Spring

As the wheel's peripheral elements undergo deflection in the contact patch, elastic forces are generated in the air springs at these positions. There are several analytical models for air springs. Considering quasi-static (low frequency) modeling, the damping associated with the air column moving between the air spring and the reservoir through the connecting orifice and frictional effects of the flexible member are negligible and only the axial stiffness of the air spring is considered. Hence the classical model of air spring is employed [53,54,56,57]

Figure 2-3 shows the equivalent mechanical model of an air spring based on the classical theory. The axial stiffness of the air spring $\mathrm{k_s}$ is modelled as consisting of the stiffness of two mechanical springs k_{s1} and k_{s2}, where k_{s1} and k_{s2} represents the stiffness components of the air spring by virtue of axial deflection and change in effective area respectively.

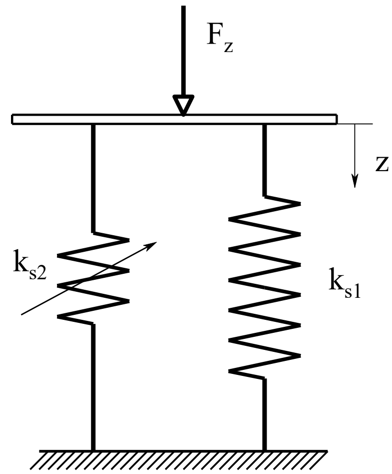

Figure 2-3 The classical model of air spring [53,56,57].

The absolute pressure inside the air spring is,

$$P_o = P_g + P_{at} \tag{2-3}$$

where P_o is the absolute pressure inside the air spring, P_{at} is the atmospheric pressure and P_g is the gauge pressure (measured pressure) inside the air spring. The elastic force in the air spring, F_a, can thus be expressed as,

$$F_a = (P_o - P_{at}) * A_e = P_g * A_e \tag{2-4}$$

where A_e, is the effective area which is different from the geometrical area. It is basically the actual area that carries the load of the air spring at an instant of operation [56]. It is a function of the pressure inside the air spring and the deflection of the air spring. For rolling lobe air springs, depending on the piston contour, the effective area can be increasing, decreasing or constant with an increasing deflection of the air spring [58].

From Eq. (2.4), the axial stiffness the air spring can be determined as,

$$k_s = \frac{dF_a}{dz} = P_g * \frac{dA_e}{dz} + \frac{dp_g}{dz} * A_e = P_g * \frac{dA_e}{dz} + \frac{dP_o}{dz} * A_e \tag{2-5}$$

The polytropic equation of state for the gas inside the air spring is given by,

$$P_o V^N = constant \qquad 2\text{-}6$$

where N is the polytropic index and V is the volume of the air spring. Differentiating Eq. (2.6) yields,

$$\frac{d}{dz}(P_o V^N) = P_o\, N\, V^{N-1}\frac{dV}{dz} + \frac{dP_o}{dz}V^N = 0 \qquad 2\text{-}7$$

For a compressive deflection of the air spring which results in a negative change in volume, and a positive change in pressure, we can write,

$$\frac{dV}{dz} = -A_e \qquad 2\text{-}8$$

Hence considering Eq. (2.7) and Eq. (2.8), an expression for the change in absolute pressure with respect to deflection can be obtained as,

$$\frac{dP_o}{dz} = \frac{N\, P_o A_e}{V} \qquad 2\text{-}9$$

Substituting Eq. (2-9) into Eq. (2-5), the axial stiffness of the air spring can be described as,

$$k_s = \frac{N P_o A_e^2}{V} + p_g\frac{dA_e}{dz} = k_{s_1} + k_{s_2} \qquad 2\text{-}10$$

thus, the axial spring rate of the air spring is a combination of its effective area change, and pressure change with deflection. Assuming that the change in effective area with deflection for the air spring is very small, then $\frac{dA_e}{dz} = 0$. Since the study is concerned with quasi-static analysis and the frequency of excitation is very small, the process inside the air spring can be considered as an isothermal process, thus resulting in a polytropic index N=1 [56].

Using Eq. (2-10), the static stiffness of the air spring can thus be expressed as,

$$k_s = \frac{P_o A_e^2}{V} \quad \text{2-11}$$

2.5 Load Carrying Mechanism of the MPW

Let us consider MPW with eight radially located airbags as shown in Figure 2-4 which are connected through rigid reservoir, placed around the rim and initially charged to a pressure of P_o. This is the unloaded charge pressure of the wheel. When the wheel is placed on the ground, and a vertical load F_z is applied through its center of gravity, the wheel deforms at the region of contact with the ground and forms the contact patch. Corresponding to the applied load F_z, there is a deflection (compression) to air spring 1. Corresponding to this, the pressure inside the wheel volume rises to P_1. At steady state, the airbags that are outside the contact patch, will tend to expand corresponding to the increased pressure P_1. However, since they are constrained by the rigid shear band, they do not undergo any deflection. Assuming that the change in effective area of the air springs with their deflection is very small, the area of the air springs is a constant nominal value, A_o.

Mechanical work done on the wheel as it is loaded is given by,

$$W_{in,M} = F_z . \Delta z_1 \quad \text{2-12}$$

where $\Delta z_1$is the deflection of air spring 1 in the contact patch under the load F_z.

Corresponding increase in the pneumatic energy of wheel can be written as,

$$U = \sum_{i=1}^{n} P_1 . dV_i \; ; i = 1, 2 \ldots n \quad \text{2-13}$$

where *n* is the number of air spokes, dV_i is the change in volume of spoke *i*

$$U = P_1 . dV_1 = \; P_1 . (dV_2 + dV_3 + dV_4 + . \, . . + dV_8) \quad \text{2-14}$$

$$P_1 \Delta z_1 = P_1 . (\Delta z_2 + \Delta z_3 + \Delta z_4 + \ldots + \Delta z_8) \quad \text{2-15}$$

where dV_i is the volume change of an air spring and Δz_i is the corresponding axial deflection of the air spring i. Thus, if the imaginary deflections of all the airbags outside the contact patch are considered equal, using Eq. (2-15) we can write,

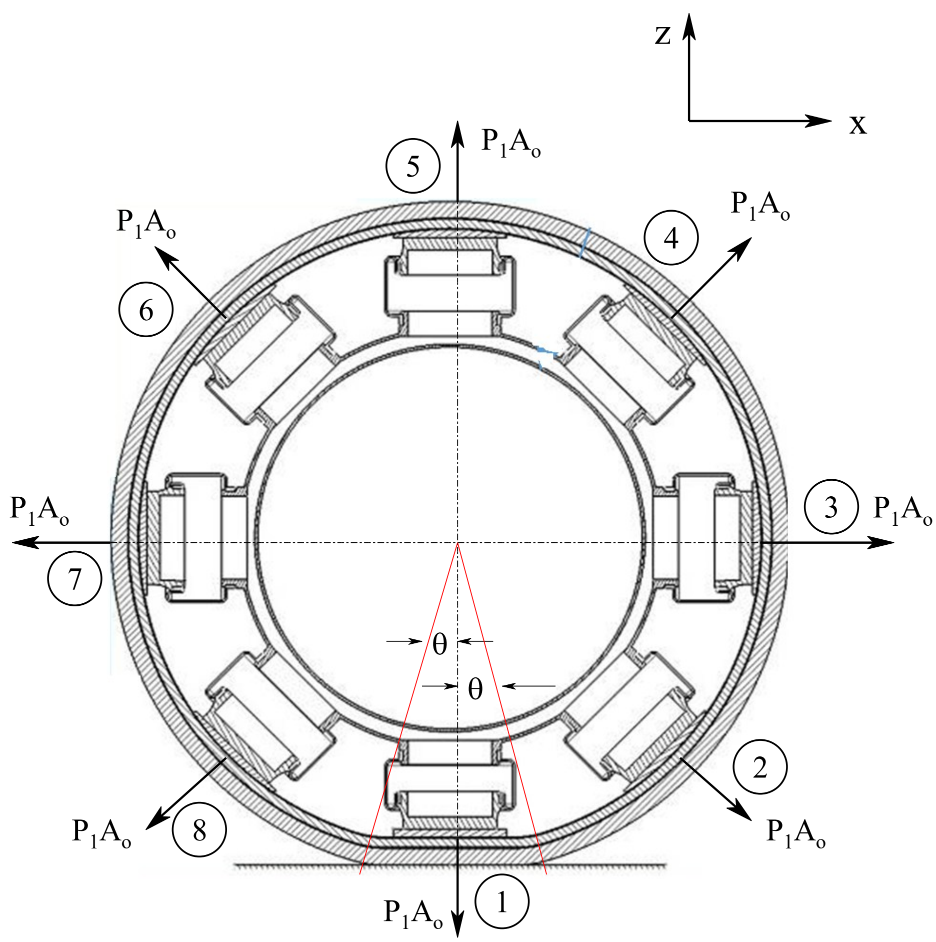

Figure 2-4 Elastic forces generated in the air springs in a loaded MPW.

$$\Delta z_1 = n_{cp} . \Delta z \quad \text{2-16}$$

where n_{cp} is the number of air springs undergoing deflection outside the contact patch. Hence the imaginary deflection of air springs outside the contact patch is given by,

$$\Delta z = \frac{\Delta z_1}{n_{cp}} \tag{2-17}$$

2.6 Equivalent Vertical Stiffness of the MPW.

From Figure 2-4, the applied vertical load of the MPW, F_z is balanced by the resultant of the vertical components of the elastic forces generated in all the air springs, F_v.

$$F_v = \sum_{i=1}^{n} F_{a,i}\, cos\theta_i \tag{2-18}$$

where $F_{a,i}$ is the axial elastic force generated by the i^{th} air spring. For the air spring, $F_{a,i} = k_i . \Delta z_i$, then Eq. (2-18) yields,

$$F_v = \sum_{i=1}^{n} k_i . \Delta z_i cos\theta_i \tag{2-19}$$

where k_i is axial spring rate of air spring *i* and θ_i is its angular position.

Considering the change in effective area of air springs with deflection, and using Eq. (2-8) and Eq (2-11), we may write,

$$F_v = \sum_{i=1}^{n} P_1 . A_o cos\theta_i \tag{2-20}$$

Hence, the equivalent vertical stiffness of the MPW can be obtained as,

$$K_z = \frac{F_v}{\Delta z_{max}} \tag{2-21}$$

where Δz_{max} is the deflection of the tire under the applied vertical load, F_z.

2.7 Selection of a MPW Design Configuration and its Performance Analysis

2.7.1 MPW Design Configuration Selection Based on Load Sharing

To choose the best design configuration for the MPW, the three design configurations are studied in terms of load sharing between the air springs. Good load sharing among the air springs is essential to a sound wheel design to avoid large contact forces which could lead to high stress in the contact patch and large pressure fluctuations during the operation of the wheel. The load sharing among the air springs is evaluated in terms of the change in air pressure in the air springs as the wheel is loaded and rotates quasi-statically. For one complete quasi-static revolution of the wheel with an angular velocity, ω of 1 rad/s, the steady-state pressure inside the air springs (or the working volume of the wheel reservoir, for the coupled configurations) for each step of the rotation is calculated from the gas state Eq. (2.6), for an isothermal process, N = 1. This kineto-static analysis is carried out for all three design configurations of the MPW considering 10 number of air bag springs (n = 10), the unloaded wheel radius, R = 360 mm, unloaded charge pressure, P_0 = 350 kPa and with air bag springs of nominal design diameter of $d_0 = 76$ mm (3 inches) and nominal design height of, $h_0 = 80$ mm.

Figure 2-5 shows the steady-state pressures at each step of quasi-static rotation of the MPW for an uncoupled design configuration. It illustrates the pressure variation within the individual air springs as a function of their angular position φ with respect to the wheel's vertical centerline (see Figure 2-2). In the illustration, the air spring aligned with the wheel's vertical center line at the beginning of the quasi-static rotation of the wheel and located within the center of the contact patch at φ =0 radian, undergoes maximum deflection, and is denoted as air spring 1. The consecutive air springs are labelled in ascending order in the counterclockwise direction. Each air spring exhibits large, identical pressure increases sequentially as it encounters the ground contact. As each air spring exits the contact patch, the pressure falls back to the initial unloaded charge pressure, P_0. The fluctuation of pressure in the air springs in the contact patch does not influence the pressure in the air springs outside the contact patch. The maximum pressure variation in each air spring is of the order of 90 kPa from the static charge pressure of 350 kPa. The uncoupled air springs thus do not share any load amongst them. The wheel load is supported only by those air springs that undergo deflection at the instant of revolution in the contact patch and the wheel acts as a bottom loader. This design configuration may lead to large deflections of the air springs in the contact patch resulting in high contact pressure and large oscillations in the wheel-ground contact force. Hence such a design is not considered feasible.

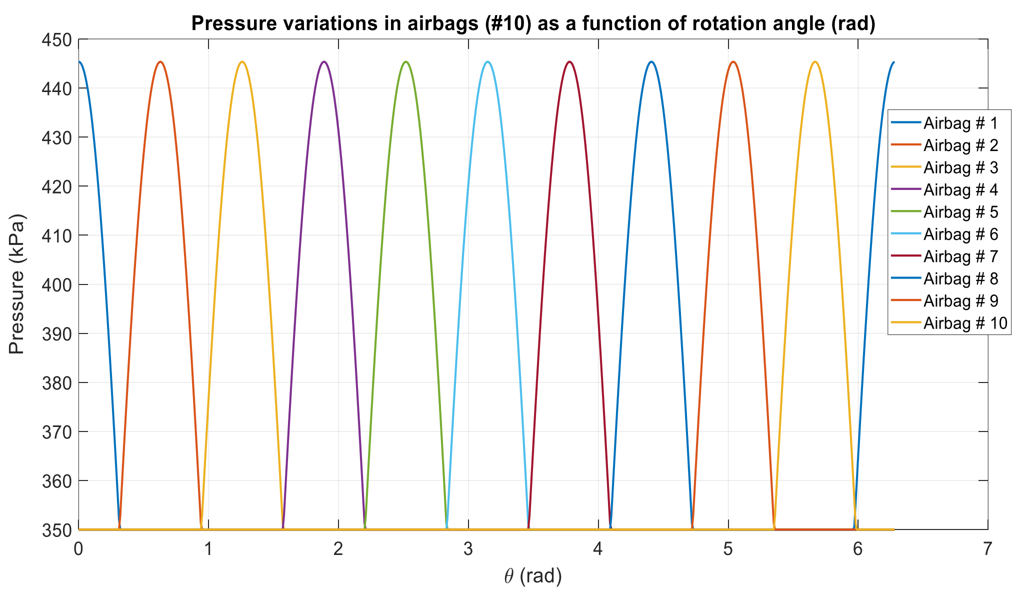

Figure 2-5 Variation in gas pressure in the individual air springs during one complete revolution of the MPW with uncoupled air springs.

Figure 2-6 shows the pressure variation within the individual air springs as a function of their angular position φ with respect to the wheel vertical centerline for the series coupled design configuration of the MPW. The air springs in the contact patch exhibit maximum pressure variations of the order 90 kPa when aligned with the wheel vertical axis, inside the contact patch. Unlike the uncoupled configuration, each air spring in the series connected design exhibits changes in pressure during the entire revolution of the wheel. In other words, the fluctuation of pressure in the air springs in the contact patch influences the pressure in the air springs outside the contact patch. The peak pressure within an air spring gradually diminishes with the wheel rotation as it rotates out of the contact patch. As an example, Figure 2-7 illustrates variations in the pressure in one air spring, #5. The pressure of gas in this air spring approaches a peak value of about 445 kPa when it aligns itself with the wheel's vertical axis, inside the contact patch at φ =0 radian. The gas pressure, however, gradually diminishes as it moves away from centre of the contact patch. This is due to the flow of air to and from the adjacent air springs #4 and #6. The series-coupled air springs thus permit some degree of load sharing among them. There is however still a substantial pressure fluctuation within each air spring which would cause considerable contact pressure and oscillations in the wheel-ground contact force. Although the amplitude of oscillations could be reduced to an extent by increasing the number of air springs in the MPW, this would require using air springs of smaller nominal diameter, resulting in a smaller wheel working volume, leading to relatively higher vertical stiffness of the MPW. Consequently, the series coupled design configuration is also judged as infeasible.

Figure 2-8 shows the pressure variation within the individual air springs as a function of their angular position φ with respect to the wheel vertical centerline for the parallel coupled design configuration of the MPW. Owing to the direct coupling of the air springs with the central reservoir, identical gas pressure is achieved for all the air springs and the reservoir. Although individual air springs have different magnitudes of deflection, at the steady-state condition, identical pressure is achieved in all the air springs. This indicates perfect load sharing among all the air springs. The parallel coupled configuration also shows substantially lower fluctuation in the pressure, in comparison with those of uncoupled and series-coupled configurations. The parallel coupled configuration can thus lead to more uniform contact pressure and wheel-ground contact force. The results suggest that the amplitude of oscillation of the gas pressure variation can be reduced by increasing the number of air springs. The MPW design configuration with parallel coupled air springs is thus selected as the feasible design configuration for the MPW.

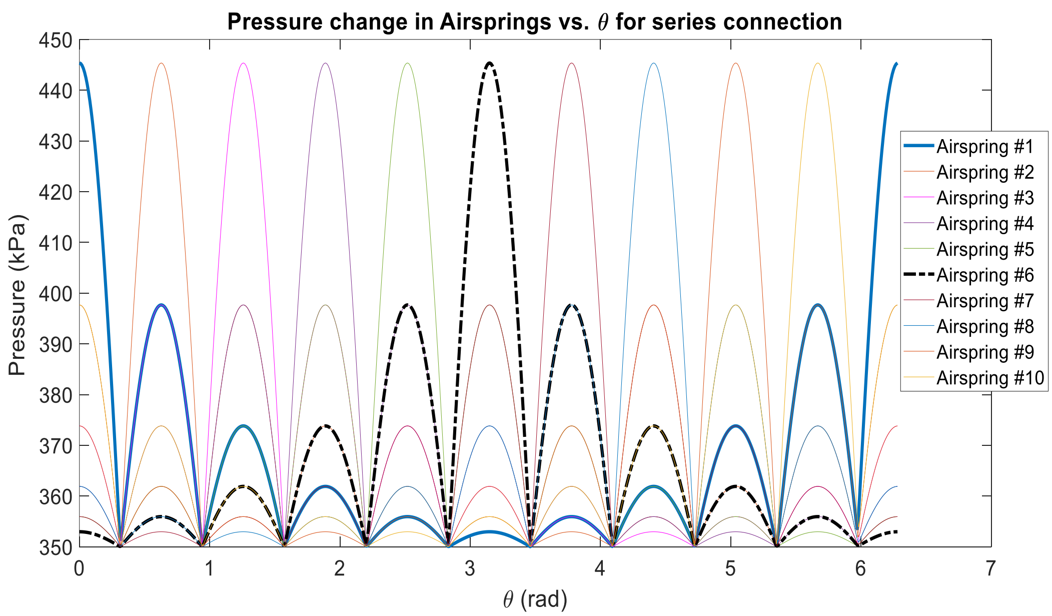

Figure 2-6 Variation in gas pressure in the individual air springs during one complete revolution of the MPW with series coupled air springs.

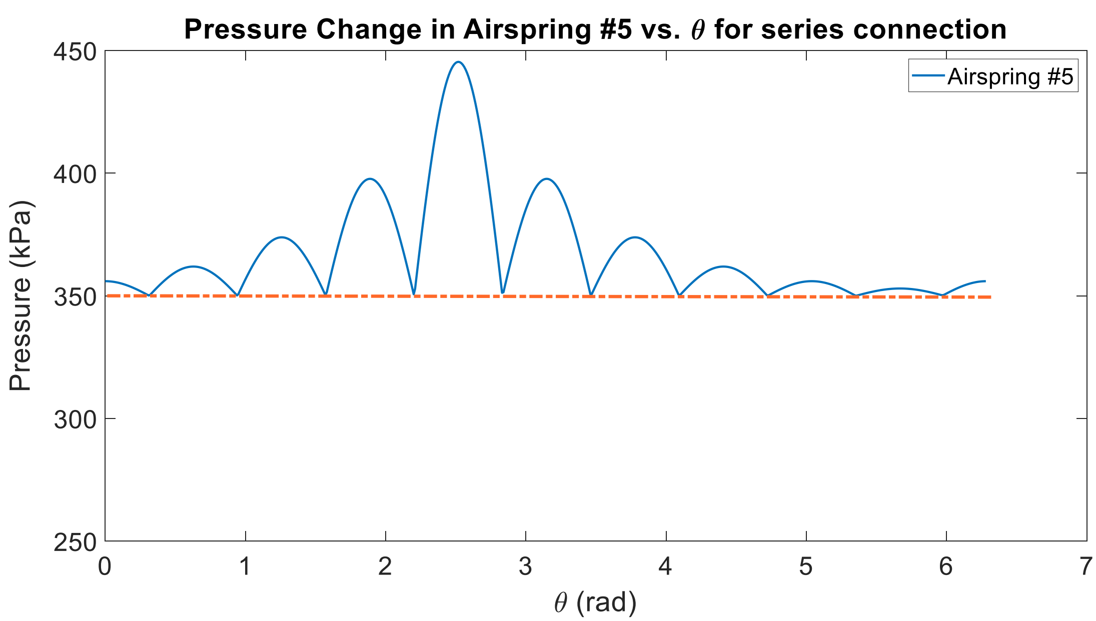

Figure 2-7 Variation in gas pressure in air spring #5 as a function of its angular position.

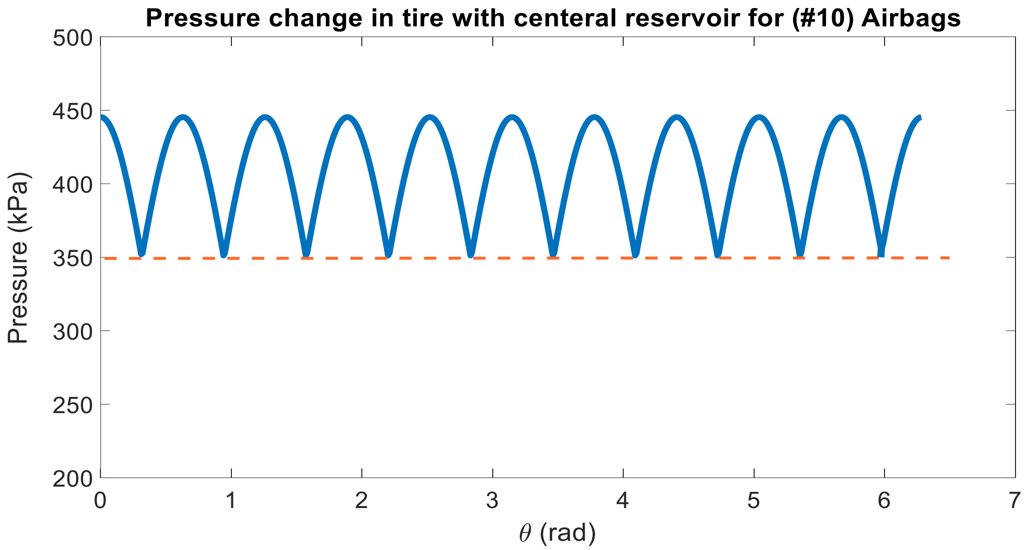

Figure 2-8 Variation in gas pressure in the individual air springs (and wheel volume) during one complete revolution of the MPW with parallel coupled air springs.

2.7.2 MPW Design Targets and Dimensions

Following the selection of the parallel coupled design configuration for the MPW, its specific design constraints and targets are established considering a reference pneumatic tire (205/55R16) as provided in Table A-1, and the honeycomb NPW, which are summarized in Table 2-1. The reservoir for the parallel-coupled design configuration was assumed to be a 0.2 m wide and 0.01 m high rectangular cross-sectioned tube around the wheel rim. Under a given static charge pressure and reservoir volume, the size and number of the air bag springs constitute the primary design factors for achieving a target load-carrying capacity or stiffness for the MPW. The target vertical stiffness can be realized by varying the number and dimensions of the airbags, and the reservoir volume. Assuming a fixed reservoir volume of 0.0002 m3, the target vertical stiffness can be realized by selecting an adequate number and dimensions of the airbags. The rim radius is permitted to vary depending on the height of the airbag. A wheel design with a larger number of airbags is considered beneficial for realizing more uniform ground-wheel contact force distribution and less gas pressure oscillation in air bags. The number of airbags, however, is constrained by the diameter

Table 2-1 Design constraints and targets for the MPW

Design constraints and targets	values	notes
Overall wheel radius, R	0.316 m	*
Rim radius, $\boldsymbol{r_0}$	0.178 m – 0.279 m	*
Maximum wheel deflection under nominal load	0.0158 m	*
Static loaded radius, $\boldsymbol{R}^*$	0.3 m	*
Tread Thickness	0.01 m	chosen
Sandwiched shear band thickness	0.0105 m	chosen
Reservoir volume	0.0002 m^3	chosen
Half-contact patch angle	18.88°	*
Reference inflation pressure	220 kPa	*
Load carrying capacity at the reference inflation pressure	3 kN	*
Maximum tire deflection at the reference inflation pressure for the max load	0.0158 m	*
Equivalent Vertical stiffness	190 kN/m	*

of the airbag and the height of the airbag that determines the rim circumference. The elliptical cross-section airbags with a major diameter as large as the wheel width and substantially smaller minor diameter are also considered to accommodate a larger number of airbags.

Table 2-2 Sizes and number of airbags considered for the MPW design.

Air-spring Cross-section	Dimension (in x in)	Number of air springs	Design height (mm)
Circular	3×3	12, 15, 18, 20	36, 42.5, 50.3, 55.3
	4×4	12, 15	59.4, 72
	5×5	12	90

Depending on the diameter of the airbags, different combinations of number of air bags and their design height is possible. Table 2-2 summarizes the cross-section dimensions and design height together with number of the airbags that could be incorporated in wheel design for airbags of circular cross-sections. The chosen size and number ofairbags would also satisfy the target load-carrying capacity and the vertical stiffness of the MPW.

2.7.3 Performance Analysis: Load-carrying Capacity and Vertical Stiffness

Kineto-static study is again carried out on the feasible, parallel design configuration of the MPW, to investigate the variation in its normal load and equivalent vertical stiffness in a quasi-static condition. The variations in these two performance measures should ideally be minimal, irrespective of the air springs' design parameters. The quasi-static model of the wheel is analyzed to determine variations in wheel load and equivalent vertical stiffness for different dimensions and numbers of airbags. The nominal wheel load is considered as 3 kN, while the target vertical stiffness is 190 kN/m, as summarized in Table 2.1. Figure 2-9 shows the variations in the equivalent vertical stiffness and normal load of the wheel with 3-inch diameter airbags as a function of the angular position of the wheel. The results are presented for different numbers of spokes (12, 15, 18 and 20). Results show the mean vertical stiffness in the order of the target stiffness (190 kN/m), while the mean normal load is also 3kN. The results also show notable variations in the normal load and stiffness. The largest variations are evident for the wheel design with n =12, which diminishes with increasing the number of spokes.

Figure 2-10 and Figure 2-11 show the variations in equivalent stiffness and normal load of the wheel design with 4 in and 5 in diameter spokes, respectively, and n =12 and 15. The results show similar variations in the stiffness and the normal load while wheel design with 15 air bags having 4-in diameters having minimal variation in the vertical stiffness and load carrying capacity. Results generally show that the variations in the normal load and the stiffness are very small, irrespective of the number and size of the spokes. The addition of an elastic tread to the wheel is expected to further reduce such variations.

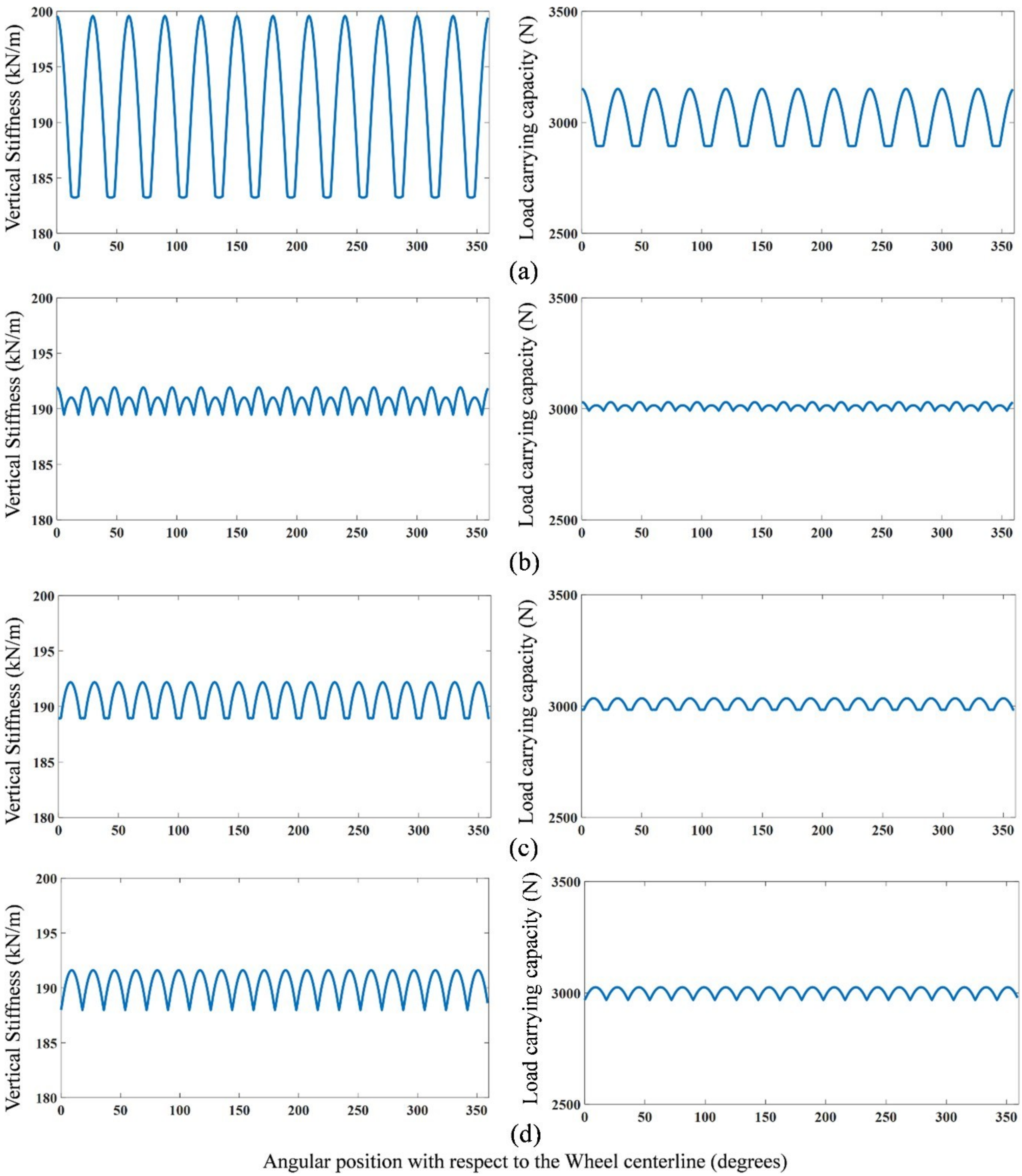

Figure 2-9 Variations in equivalent vertical stiffness (left column) and normal load (right column) during one complete revolution ofthe MPW with 3 in diameter spokes: (a) n=12; (b) n=15; (c) n=18; and (d) n=20.

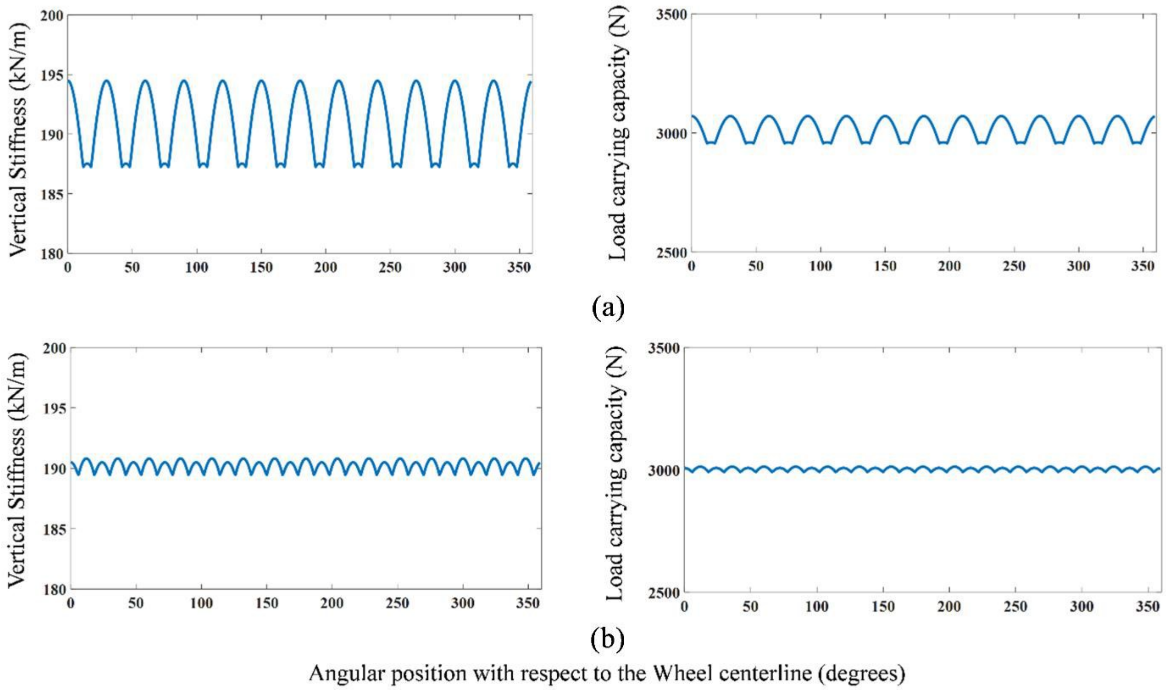

Figure 2-10 Variations in equivalent vertical stiffness and normal load during one complete revolution of the MPW with 4 in diameter spokes: (a) n=12; and (b) n=15.

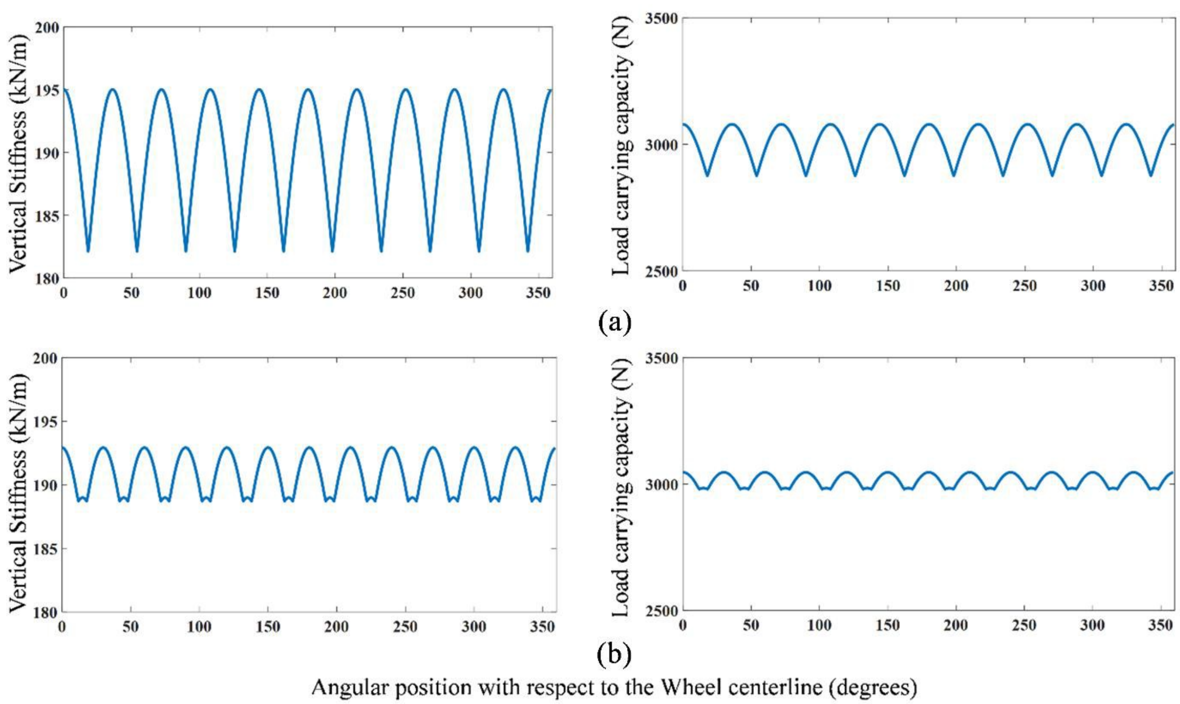

Figure 2-11 Variations in equivalent vertical stiffness and normal load during one complete revolution of the MPW with 5 in diameter spokes: (a) n=12; and (b) n=15.

2.8 Quasi-static Model of the MPW with Tread

The observed fluctuations in the wheel's air pressure and thus the contact force can be partly suppressed bythe addition of a relatively soft tread to the shear ring. The quasi-static model of the MPW, described in section 2.3, can be effectively utilized to investigate the effect of tread. Figure 2-12 illustrates the radial deflection of a non-rotating wheel with an elastic tread over half of the contact patch.

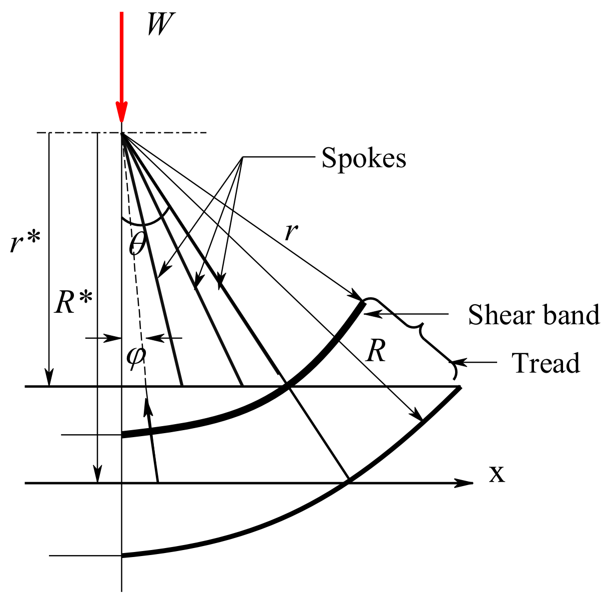

Figure 2-12 Geometrical representation of the half-contact patch with the tread and the radial displacement of the pneumatic spokes.

The wheel load W imposed on the rim center is supported by the radially distributed spokes and the tread within the contact region. It is assumed that the tread within the half contact patch couldbe modelled as m discrete radial spring elements with identical stiffness k, as shown in Figure 2-12. The spring element positioned at the vertical axis of the wheel (x = 0) is numbered as i = 0 and that at the end of the contact patch is numbered as i = m. It is noted that in Figure 2-13, R^* and R are the loaded (deformed) and unloaded (un-deformed) radii of the wheel including the tread, respectively,and r^* and r represent the loaded (deformed) and unloaded (un-deformed) radii of the shear band (outer surface), respectively. The independent variable x denotes the position of each point in thecontact patch with respect to the wheel vertical axis. θ is the angle of half contact patch, and φ the angular position of each spring element (tread) with respect to the vertical axis. ($R - f$ (x, φ)) denotes the radial displacement of each point on the outer surface of the tread. Similarly, $r - g\ (x, \varphi)$ is the radial displacement of each point on the shear band, which also describes the deflection of the pneumatic spokes within the contact region. $R - f\ (x, \varphi)$, φ and θ can be determined from the following geometric relations,

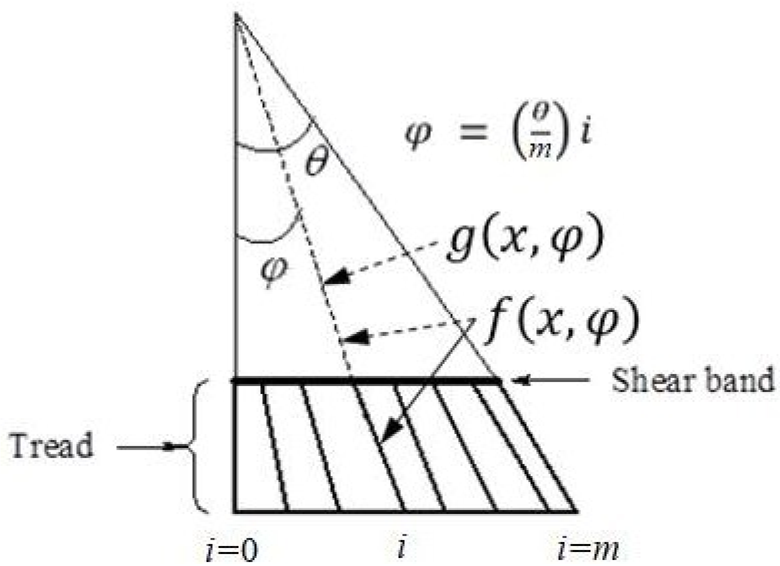

Figure 2-13 The tread modelled as a set of discreet springs.

$$cos\varphi = \frac{R^*}{f(x,\varphi)} \qquad 2\text{-}22$$

$$cos\,\theta = \frac{R^*}{R} \qquad 2\text{-}23$$

$$R \text{ - } f(x,\varphi) = R(1 - \frac{cos\theta}{cos\varphi}), \quad where\ {-\theta} < \varphi < \theta \qquad 2\text{-}24$$

Similarly, $r - \ g(x,\varphi) = r(1 - \frac{cos\theta}{cos\varphi})$, where $-\theta < \varphi < \theta$ 2-25

The deflection of i^{th} spring element in the tread, δ_{ti}, is thus determined from,

$$\delta_{ti} = (R-r)\left(1-\frac{cos\theta}{cos\varphi}\right), \qquad \varphi = \left(\frac{\theta}{m}\right)i \tag{2-26}$$

The effective stiffness of the tread, K_t, can be calculated from the spring rate of individual springelement, as,

$$K_t = 2k\sum_{i=0}^{m} cos(i\frac{\theta}{m})^2 \tag{2-27}$$

The local force (radial) developed in the ith spring element of the tread, F_{ti}, together with its global vertical component can be expressed as,

$$F_{ti} = k\delta_{ti} = k \times \left\{\left(1-\frac{cos\theta}{cos\left(\frac{\theta}{m}\right)i}\right)(R-r)\right\} \tag{2-28}$$

The net vertical components of the spring forces, F_{tz}, supporting the wheel load (W) may thus bedetermined as,

$$F_{tz} = k\sum_{i=0}^{m}\left\{\left(1-\frac{cos\theta}{cos\left(\frac{\theta}{m}\right)i}\right)(R-r)\right\} \tag{2-29}$$

The equivalent vertical stiffness of the MPW (K_{eq}) is obtained considering series combinations of two springs, which represent the equivalent stiffness of the radially oriented air springs (Kz) and the tread (Kt), as illustrated in Figure 2-14. The equivalent vertical stiffness of the MPW model with the tread is thus obtained as,

$$K_{eq} = \frac{Kz \times Kt}{Kz + Kt} \tag{2-30}$$

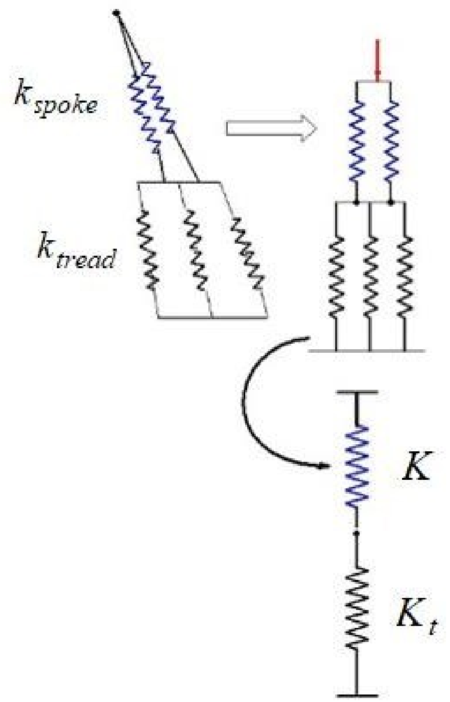

Figure 2-14 K_{eq} of The MPW as the equivalent stiffness of K_z and K_t

2.9 Parametric Study of the MPW

To understand the relation between the design variables and the equivalent vertical stiffness of the wheel and pressure fluctuation within the wheel, a parametric study is carried out. The design variables in the parametric study are diameter of the air bags, *D*, number of air bags, *n*, and the design height of the air bags, h_0. The charge pressure of the wheel, P_0 and the reservoir volume V_0 are both fixed for the parametric study and hence are considered as design input parameters. Through the parametric study, a set of reasonable values of the design variables which meets the target equivalent vertical stiffness of the wheel, 190 kN/m while also providing a low-pressure fluctuation within the wheel of the MPW were obtained.

At a fixed charge pressure, P_0 of 220 kPa, and reservoir volume V_0, of 0.0002 m^3, for each diameter of the airbag, *D*, varying the number of bags, *n* for different combinations of the height of the bags, h_0 were studied to find the combinations that would give the best target performance measures. To maintain the specified wheel size, as the design height of the bags vary, the rim size is considered as a variable with a lower bound of 0.178 m and an upper bound of 0.279 m as provided in table 2-1. The key design variables are thus identified as n, D and h_0. The trend in the variation of the vertical stiffness and pressure fluctuation, with these key control variables was verified with the formulations for the vertical stiffness of the MPW. Subsequently, the combinations of n, D and h_0 for each diameter of air bags, that gave the target vertical stiffness with a sufficiently good amount of load sharing between the bags in terms of low-pressure fluctuations were selected as the suggested design variables combinations for the optimization study of the MPW.

2.10 Optimization Study of the MPW

Following the parametric study where the key design variables of the MPW for the target performance measures of the wheel were identified, an investigation on finding optimal combinations of the key design variables for the MPW, at a fixed reservoir volume, V_0 was carried out. This optimal combination of the key design variables was found for the target stiffness of the MPW, K = 190 kN/m. The optimization problem was thus formally formulated as:

Find the design vector $X = \{P_0, D, h_0\}$,

to minimize the objective function, $U(X) = \left|\frac{K}{190} - 1\right|$,

Subjected to following side constraints,

$0.0762 \text{ m (3 in)} \leq D \leq 0.127\text{m (5 in)}$,

$0.0166 \text{ m} \leq h_0 \leq 0.1182 \text{ m}$,

$200 \text{ kPa} \leq P_0 \leq 300 \text{ kPa}$,

and limit on the variation of vertical stiffness as,

$\frac{\Delta K}{K} \leq 0.5$ %,

The optimization problem ahs been solved using MATLAB optimization toolbox. Genetic Algorithm (GA) is initially used to identify the near global optimum solutions. Results from GA were then used as the initial point for the gradient based optimization algorithm, sequentially quadratic programming technique (SQP), in fmincon tool in MATLAB optimization toolbox to capture accurate global optimum solution. It is noted that the gradient based optimization algorithms are capable of accurately capturing local optimum solution. Thus, combination if GA and fmincon can results to an accurate global optimum solution. Results how that irrespective of different optimum values from GA (population size of 100), the combination of GA and SQP converged to a unique solution. Table 2-3 provided the optimum solution for design variables D and h_0 for different combinations of charged pressure, P_0, and number of airbags, *n*.

Result show that to maintain a constant equivalent stiffness of 190 kN/m, for the n = 15 as charge pressure increases, the design height of the air bags increases while the design diameter decreases. It is noted that the diameter term is in the power of two in the stiffness equation ($k = \frac{PD^2}{h0}$). For n = 18, however the height of air bags increases up to charge pressure of 260 kPa and then decreases with further increase in charge pressure while the diameter decreases with increasing pressure with the same slope. For n = 20, a configuration with higher number of bags, the design height and design diameter generally decrease with an approximately same slope by increasing the charge pressure.

Table 2-3 Optimal combination of D and h_0 values for different values of P_0 and n

n	P_0 (kPa)	h_0(mm)	D (mm)	U (X)	$\frac{\Delta K}{K} \times 100$
15	200	50.637	87.05088	2.25E-08	3.14E-03
	220	55.417	87.16518	2.12E-08	1.76E-03
	240	47.522	76.76134	9.87E-08	6.44E-04
	260	58.612	82.64144	3.70E-07	6.69E-04
	280	54.165	76.32446	3.17E-07	2.89E-04
	300	59.886	77.83068	2.37E-07	1.70E-05
18	200	82.977	103.3907	1.46E-07	5.25E-04
	220	87.583	101.40442	2.87E-08	1.10E-03
	240	96.311	102.01148	5.80E-07	6.80E-04
	260	103.220	101.60000	3.51E-07	6.97E-03
	280	90.024	91.18600	7.57E-07	1.78E-03
	300	80.729	83.21802	1.37E-07	2.71E-03
20	200	90.097	102.39502	3.59E-07	3.67E-04
	220	75.591	89.05494	2.62E-08	2.56E-03
	240	67.981	80.61960	1.34E-07	2.81E-03
	260	67.010	76.86802	5.15E-08	1.02E-03
	280	73.831	77.97038	4.03E-07	3.03E-03
	300	75.511	76.22540	3.58E-10	3.03E-03

2.11 Summary

This chapter details the conceptualization and analysis of the Mechano-Pneumatic Wheel (MPW), an innovative hybrid tire design concept, combining the benefits of pneumatic and non-pneumatic tire technologies. The MPW is built on radially arranged air springs supported by a composite shear band and tread. The chapter explores three coupling configurations for the air springs uncoupled, series-coupled, and parallel-coupled, to identify the optimal configuration for load sharing and minimizing pressure fluctuations. An analytical quasi-static model is developed to estimate vertical stiffness and load carrying mechanism of the wheel. The parallel-coupled

configuration is identified as the most feasible due to its reduced pressure fluctuations, offering significant performance advantages over alternative designs. To refine the MPW's design parameters, a detailed parametric study and optimization evaluates the effects of number of air springs and their dimensions as well as charge pressure. The results indicate that the MPW meets its target stiffness of 190 kN/m, demonstrating its viability as a robust, low-maintenance, and sustainable alternative to conventional tire systems. This chapter establishes the foundation for a design that addresses critical challenges in tire performance and durability.

Chapter 3. Modeling the Shear Band

3.1 Introduction

Along with the air springs, another load-carrying member in an NPT that replaces the inflation pressure in a Pneumatic Tire is the Shear band [2,59]. The shear band is a circular beam that deforms primarily in pure shear [34]. It consists of a ring made of a low-shear modulus material, like polyurethane [2,32,59] reinforced by sandwiching between two inextensible membranes [2], like Aluminium alloy [34] or High-Strength Steel [59]. It is a composite structure that holds the flexible spokes, makes contact the ground, and keeps the shape of the NPT [59].

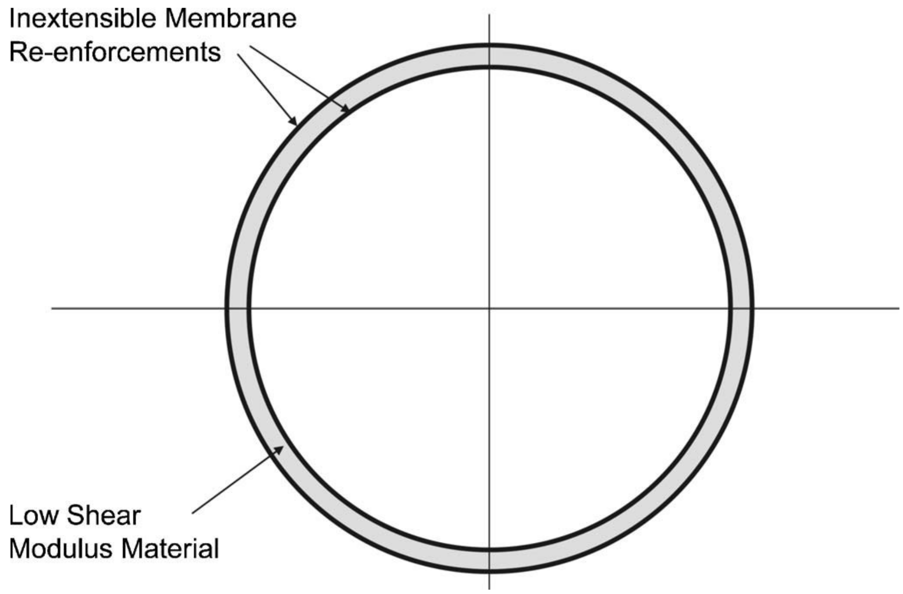

Figure 3-1 Structure of Shear band.

Since its invention the shear band was quickly adapted as a design of choice for NPTs in lieu of the inflation pressure in Pneumatic tires. This success of the shear band is accounted by it possessing the four critical characteristics of a Pneumatic tire: low contact pressure, low stiffness, low mass and low energy loss on impact with obstacles. without the inflation pressure [2].

3.2 Analytical Model of the Shear Band

The analytical modeling of the shear band serves as a foundational approach to understanding its mechanical behavior under load, particularly in non-pneumatic wheels (NPWs). To accurately represent the load bearing and deformation characteristics of the shear band, it is modeled as a curved Timoshenko beam. This model captures critical aspects of shear band behavior, including bending, axial stretching, and transverse shear deformations, which are often overlooked in simpler beam theories. This section explores the contact mechanics of a uniformly curved beam interacting symmetrically with a flat, rigid surface, emphasizing the contact stress distribution normal to the surface. The analysis assumes in-plane deformation, simplifying the 3-D elastic continuum into an equivalent 1-D beam representation. A beam with uniform rectangular cross-section is considered, with constant width, thickness, and a radius of curvature defined at the centroid of the cross-section. The Timoshenko beam model's governing equations and boundary conditions are outlined, providing a framework for understanding the shear band's structural performance under operational conditions.

3.2.1 Shear Band Modeled as a Curved Timoshenko Beam.

In the original model of the MPW, the only load carrying members considered in the study were the rolling lobe air springs. However, in an NPW the load is carried by both the air springs and the Shear band. To understand the effect of the shear band on the performance of the MPW, the shear band is modelled as a curved Timoshenko beam. Modeling the shear band using Timoshenko beam theory allows for a comprehensive analysis, capturing the bending, shear, and axial deformations relevant to its performance under load. The Timoshenko beam theory is selected over simpler beam models to address both bending and transverse shear deformations, which are essential in modelling the flexible but load-bearing characteristics of the shear band. This theory introduces three stiffness parameters:

Axial stiffness (EA) that determines the resistance to axial stretching along the shear band, impacting load-carrying capacity, bending stiffness (EI) governs the resistance to bending deformations perpendicular to the shear band's plane and the Shear stiffness (GA) which accounts for resistance to transverse shear deformation, an important factor in thick beams or materials like the NPT shear band. This section presents the theoretical formulation, strain-displacement relationships, boundary conditions, Simulink model setup, and insights from finite element analysis validation. A set of three coupled, second order governing differential equations are obtained for the behaviour of the shear band in the contact region. The governing equations are solved for the radial displacement u_r, circumferential displacement u_θ, and rotation of the beam cross-section ϕ. The resulting displacement field is validated through FEA results of a 2-D circular ring. This study examines the symmetric contact between a uniformly curved beam and a flat, rigid surface, focusing on the contact stress normal to the rigid plate. The governing equations and solutions are dependent on the three fundamental stiffness parameters: EA, EI, and GA. [39,40].

Figure 3-2 (a) depicts a uniformly curved beam of a uniform rectangular cross-section. b is its constant width, h is its constant thickness, and R denotes the radius of curvature of the centroid of the cross-section [39,40]. The analysis considers only in-plane deformation, with the 3-D elastic continuum being represented as a 1-D beam, as depicted in Figure 3-2 (b) [39,40].

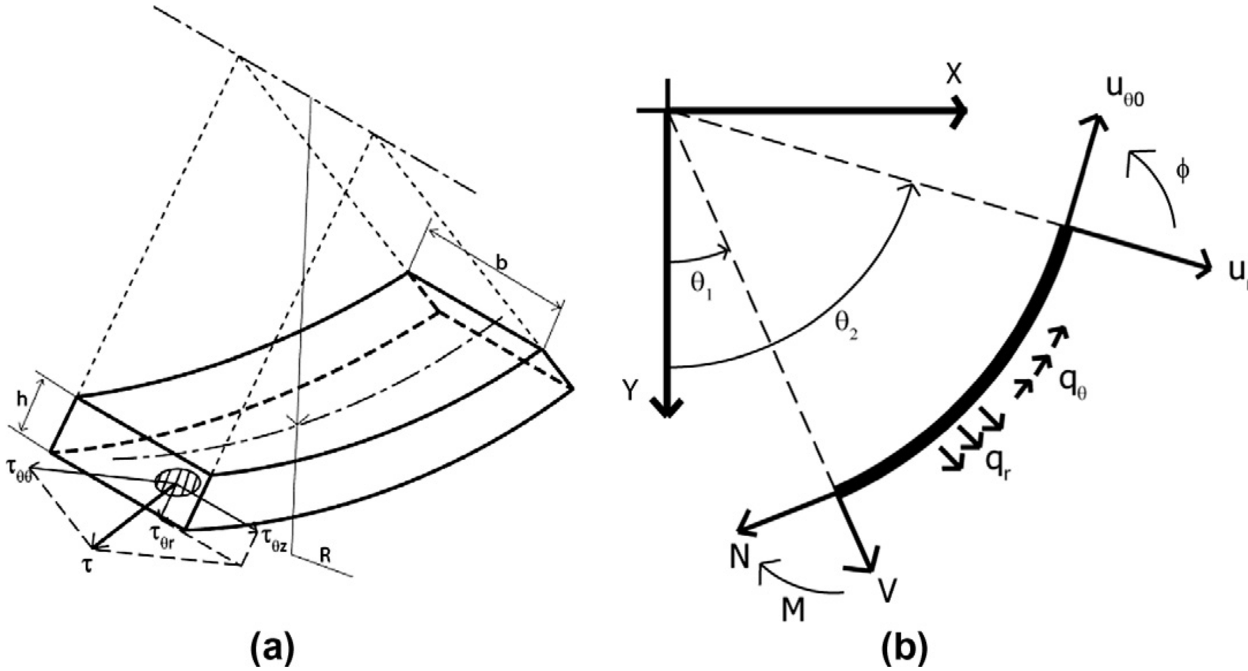

Figure 3-2 Uniformly curved, rectangular cross sectioned Timoshenko beam cross section. (a) Out of plane deformation in 3-D, (b) In plane deformation in 2-D [39,40]

3.2.2 Equilibrium Equations of the Shear Band

In accordance with Timoshenko beam theory, it is assumed that the beam's cross-section rotates while remaining straight after deformation, implying uniform shear strain and, consequently, uniform shear stress throughout the thickness [39,40]. The corresponding displacement field is given by,

$$\begin{aligned} u_r(r,\theta) &= u_r(R,\theta) = u_r(\theta) \\ u_\theta(r,\theta) &= u_{\theta 0}(\theta) + (r-R)\phi(\theta) \end{aligned} \tag{3-1}$$

where, $u_r(\theta)$ is the transverse displacement, $u_\theta(\theta)$ is the circumferential displacement, and $\phi(\theta)$ is the cross-section rotation with respect to the centroid of the cross-section [39,40]. By introducing the thickness variable $Z = r - R$, the displacement field is expressed as,

$$\begin{aligned} u_r(z,\theta) &= u_r(\theta), \\ u_\theta(z,\theta) &= u_{\theta 0}(\theta) + Z\phi(\theta). \end{aligned} \tag{3-2}$$

Substituting Eq. (3-2) into the standard expressions for strain in polar coordinates gives,

$$
\begin{aligned}
&\varepsilon_{rr} = \frac{\partial u_r}{\partial r}, \\
&\varepsilon_{\theta\theta} = \frac{1}{r}\frac{\partial u_\theta}{\partial \theta} + \frac{u_r}{r}, \\
&\gamma_{r\theta} = 2\varepsilon_{r\theta} = \frac{1}{r}\frac{\partial u_r}{\partial \theta} + \frac{\partial u_\theta}{\partial r} - \frac{u_\theta}{r}
\end{aligned}
\tag{3-3}
$$

which gives,

$$
\begin{aligned}
&\varepsilon_{rr} = 0, \\
&\varepsilon_{\theta\theta} = \frac{1}{R+Z}\left(\frac{du_{\theta 0}}{d\theta} + u_r + Z\frac{d\phi}{d\theta}\right) \\
&\gamma_{r\theta} = \frac{1}{R+Z}\left(\frac{du_r}{d\theta} - u_{\theta 0} + R\phi\right)
\end{aligned}
\tag{3-4}
$$

The virtual strain energy for a sector of a circle, between the angles θ_1 and θ_2 as shown in Figure 3-2 is given by,

$$
\begin{aligned}
\delta U &= \int_{\Omega} (\sigma_{\theta\theta}\delta\varepsilon_{\theta\theta} + \tau_{r\theta}\delta\gamma_{r\theta}) d\Omega \\
&= \int_{\theta_1}^{\theta_2} \int_A (\sigma_{\theta\theta}\delta\varepsilon_{\theta\theta} + \tau_{r\theta}\delta\gamma_{r\theta}) r dA d\theta
\end{aligned}
\tag{3-5}
$$

Substituting Eq. (3-4) into Eq. (3-5) yields,

$$
\begin{aligned}
\delta U &= \int_{\theta_1}^{\theta_2} \int_A \Bigg(\sigma_{\theta\theta}\frac{1}{R+Z}\delta\left(\frac{du_{\theta 0}}{d\theta} + u_r + Z\frac{d\phi}{d\theta}\right) \\
&\quad + \tau_{r\theta}\frac{1}{R+Z}\delta\left(\frac{du_r}{d\theta} - u_{\theta 0} + R\phi\right)\Bigg)(R+Z) dA d\theta \\
&= \int_{\theta_1}^{\theta_2} \int_A \Bigg(\left(\sigma_{\theta\theta}\frac{d\delta u_{\theta 0}}{d\theta} - \tau_{r\theta}\delta u_{\theta 0}\right) + \left(\sigma_{\theta\theta}\delta u_r + \tau_{r\theta}\frac{d\delta u_r}{d\theta}\right) \\
&\quad + \left(Z\sigma_{\theta\theta}\frac{d\delta\phi}{d\theta} + R\tau_{r\theta}\delta\phi\right)\Bigg) dA d\theta
\end{aligned}
\tag{3-6}
$$

In terms of stress, the resultants for bending moment, axial force, and shear force are,

$$M = \int_A Z\sigma_{\theta\theta} dA$$
$$N = \int_A \sigma_{\theta\theta} dA \qquad \text{3-7}$$
$$V = \int_A \tau_{r\theta} dA$$

The virtual strain energy expression Eq. (3-6) becomes,

$$\delta U = \int_{\theta_1}^{\theta_2} \left(\left(N \frac{d\delta u_{\theta 0}}{d\theta} - V\delta u_{\theta 0} \right) + \left(N\delta u_r + V \frac{d\delta u_r}{d\theta} \right) + \left(M \frac{d\delta\phi}{d\theta} + RV\delta\phi \right) \right) d\theta \qquad \text{3-8}$$

Integrating the above by parts, the expression of the virtual strain energy is expressed as,

$$\delta U = \int_{\theta_1}^{\theta_2} \left(\left(-\frac{dN}{d\theta} - V \right) \delta u_{\theta 0} + \left(N - \frac{dV}{d\theta} \right) \delta u_r + \left(-\frac{dM}{d\theta} + RV \right) \delta\phi \right) d\theta + [N\delta u_{\theta 0} + V\delta u_r + M\delta\phi]_{\theta_1}^{\theta_2}. \qquad \text{3-9}$$

Considering that the radial and circumferential distributed loads, $q_r(\theta)$ and $q_\theta(\theta)$, are applied at the mid-surface of the beam, the external virtual potential energy can be written as,

$$\delta V = -\int_{\theta_1}^{\theta_2} (q_r\delta u_r + q_\theta \delta u_{\theta 0}) Rb d\theta. \qquad \text{3-10}$$

The principle of virtual work states that the virtual work of a deformable continuum in a state of equilibrium is zero,

$$\delta W = \delta U + \delta V = 0 \qquad \text{3-11}$$

which using Eq. (3-9) – Eq. (3-11) yields,

$$0 = \int_{\theta_1}^{\theta_2} \left(\left(-\frac{dN}{d\theta} - V - Rbq_\theta \right) \delta u_{\theta 0} + \left(N - \frac{dV}{d\theta} - Rbq_r \right) \delta u_r + \left(-\frac{dM}{d\theta} + RV \right) \delta\phi \right) d\theta + [N\delta u_{\theta 0} + V\delta u_r + M\delta\phi]_{\theta_1}^{\theta_2}. \quad 3\text{-}12$$

Eq. (3-12) is applicable for any admissible set of virtual radial and circumferential displacements, along with virtual cross-section rotations. Consequently, the static equilibrium equations for a uniformly curved Timoshenko beam with extensibility are given by:

$$\begin{aligned} &\frac{dN}{d\theta} + V = -Rbq_\theta \\ &N - \frac{dV}{d\theta} = Rbq_r \\ &\frac{dM}{d\theta} - RV = 0 \end{aligned} \quad 3\text{-}13$$

These equilibrium equations are governed by the essential/natural boundary conditions specified in Eq. (3-13).

3.2.3 Governing Differential Equations

The material behavior is now defined using the linear constitutive relations,

$$\begin{aligned} \sigma_{\theta\theta} &= E\varepsilon_{\theta\theta} \\ \tau_{r\theta} &= G\gamma_{r\theta} \end{aligned} \quad 3\text{-}14$$

where E and G can be functions of z. Substituting Eq. (3-4) into Eq. (3-7) yields the expressions for the stress resultants in terms of the displacements as follows:

$$\begin{aligned} M &= \int_A \frac{ZE}{R+Z} \left(\frac{du_{\theta 0}}{d\theta} + u_r + Z\frac{d\phi}{d\theta} \right) dA = K_1 \frac{d\phi}{d\theta} + K_{12} \left(\frac{du_{\theta 0}}{d\theta} + u_r \right) \\ N &= \int_A \frac{E}{R+Z} \left(\frac{du_{\theta 0}}{d\theta} + u_r + Z\frac{d\phi}{d\theta} \right) dA = K_2 \left(\frac{du_{\theta 0}}{d\theta} + u_r \right) + K_{12} \frac{d\phi}{d\theta} \\ V &= \int_A \frac{G}{R+Z} \left(\frac{du_r}{d\theta} - u_{\theta 0} + R\phi \right) dA = K_3 \left(\frac{du_r}{d\theta} - u_{\theta 0} + R\phi \right) \end{aligned} \quad 3\text{-}15$$

where the stiffness coefficients introduced in Eq. (3-15) are defined as follows [39,40],

$$
\begin{aligned}
K_1 &= \int_A \frac{Z^2 E}{R+Z} dA \\
K_{12} &= \int_A \frac{ZE}{R+Z} dA \\
K_2 &= \int_A \frac{E}{R+Z} dA \\
K_3 &= \int_A \frac{G}{R+Z} dA.
\end{aligned}
\qquad \text{3-16}
$$

Substituting Eq. (3-15) into the equilibrium equations, Eq. (3-13), results in the governing differential equations for the displacement fields,

$$
\begin{aligned}
&K_2 \frac{d^2 u_{\theta 0}}{d\theta^2} - K_3 u_{\theta 0} + (K_2 + K_3)\frac{du_r}{d\theta} + K_{12}\frac{d^2\phi}{d\theta^2} + RK_3\phi = -Rbq_\theta \\
&-K_3 \frac{d^2 u_r}{d\theta^2} + K_2 u_r + (K_2 + K_3)\frac{du_{\theta 0}}{d\theta} + (K_{12} - RK_3)\frac{d\phi}{d\theta} = Rbq_r \\
&K_1 \frac{d^2\phi}{d\theta^2} - R^2 K_3 \phi + (K_{12} - RK_3)\frac{du_r}{d\theta} + K_{12}\frac{d^2 u_{\theta 0}}{d\theta^2} + RK_3 u_{\theta 0} = 0
\end{aligned}
\qquad \text{3-17}
$$

In the limit where the radius, R, is much larger than the thickness, $h, R + z$ can be approximated as R, leading to the stiffness expressions Eq. (3-163-16) being simplified to the more familiar expressions for a slender beam,

$$
\begin{aligned}
K_1 &= \frac{EI}{R} \\
K_{12} &= 0 \\
K_2 &= \frac{EA}{R} \\
K_3 &= \frac{GA}{R}.
\end{aligned}
\qquad \text{3-18}
$$

Substituting Eq. (3-18) into equation. Eq. (3-17) gives the approximate governing differential equations of a uniformly curved, extensional, Timoshenko beam as below,

$$EA\frac{d^2u_{\theta 0}}{d\theta^2} - GAu_{\theta 0} + (EA + GA)\frac{du_r}{d\theta} + RGA\phi = -R^2bq_\theta$$
$$-GA\frac{d^2u_r}{d\theta^2} + EAu_r + (EA + GA)\frac{du_{\theta 0}}{d\theta} - RGA\frac{d\phi}{d\theta} = R^2bq_r \qquad \text{3-19}$$
$$EI\frac{d^2\phi}{d\theta^2} - R^2GA\phi - RGA\frac{du_r}{d\theta} + RGAu_{\theta 0} = 0.$$

The coupled differential Eq. (3-19) are subjected to the following particular essential or natural boundary conditions, at least one of which must be specified at each edge of the beam.

$$u_r(\theta_i)/V(\theta_i) = \frac{GA}{R}\left(\frac{du_r}{d\theta} - u_{\theta 0} + R\phi\right)\Big|_{\theta_i}$$
$$u_{\theta 0}(\theta_i)/N(\theta_i) = \frac{EA}{R}\left(\frac{du_{\theta 0}}{d\theta} + u_r\right)\Big|_{\theta_i} \qquad \text{3-20}$$
$$\phi(\theta_i)/M(\theta_i) = \frac{EI}{R}\frac{d\phi}{d\theta}\Big|_i ;\ i = 1,2.$$

Table 3-1 Material Properties of the Shear Band [39,40].

Material Parameters		**Geometrical Parameters**			
E (MPa)	G (MPa)	*R* (m)	*h* (m)	*b* (m)	*δ* (m)
900	5	0.31	0.02	0.2	0.0158

3.3 Analytical Solution of Governing Equations of the Shear Band

MATLAB Simulink was employed to numerically solve the system of governing differential equations and validate the shear band model. Simulink’s block-based environment allowed for the translation of each equation into a corresponding block, facilitating the interactive simulation of the system’s response. The block diagram Setup of Simulink used to solve the set of governing differential equations is shown in Figure 3-3, defining relationships between the radial, transverse, and rotational displacements. The solver settings in Simulink were optimized for the system’s stiffness, ensuring accurate simulations of the shear band's response under various loads. The solver settings in Simulink were optimized for the system's stiffness, ensuring accurate simulations

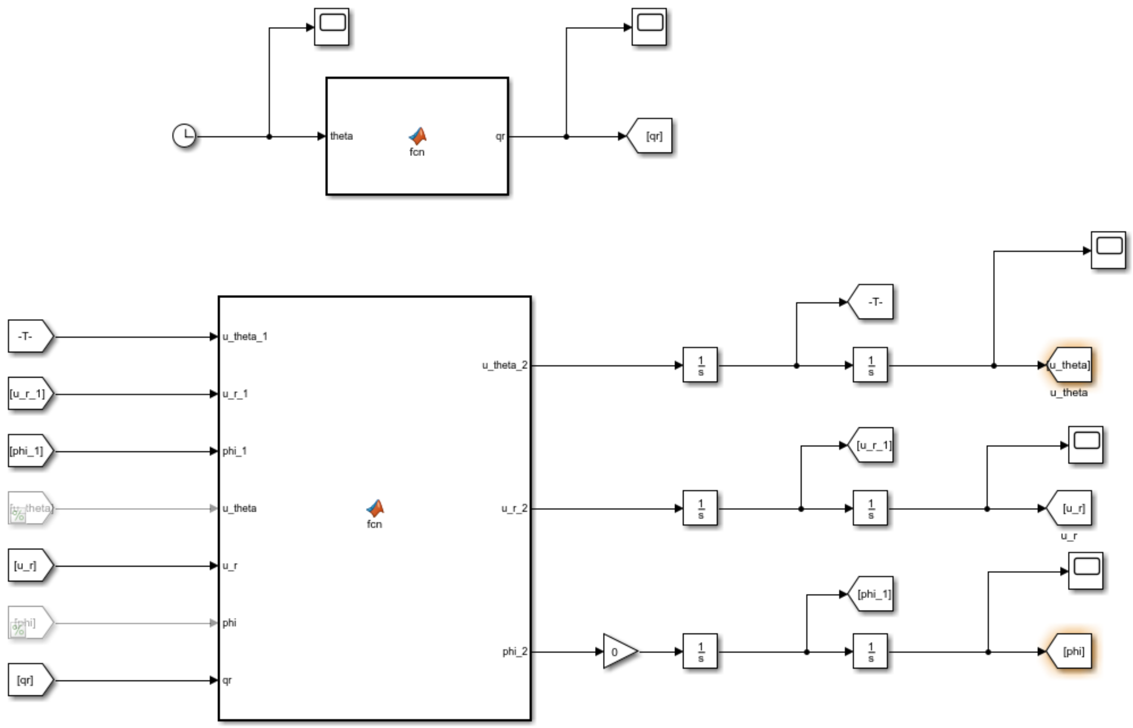

Figure 2-3 Simulink Block of the numerical solution of the Governing differential equations of the Shear band model

of the shear band's response under various loads. The model parameters, such as EA, EI, and GA, were input as tunable parameters, allowing for sensitivity analysis and exploration of optimal configurations. During the output Analysis, the simulation provided deformation profiles for varying loading scenarios, helping visualize the impact of design changes.

3.4 Validation of the Analytical Solution with FEA

The numerical solution of the governing equations of the curved Timoshenko beam model of the shear beam in equations 3-19 must be validated. For this purpose, the set of three coupled differential equations was initially solved in MATLAB Simulink as an initial value problem. The analytical results of the displacement field were then validated against a Finite Element Model of the shear beam in ANSYS Mechanical. The results were found to be in excellent agreement and hence the governing equations for the curved Timoshenko beam in the contact region are validated.

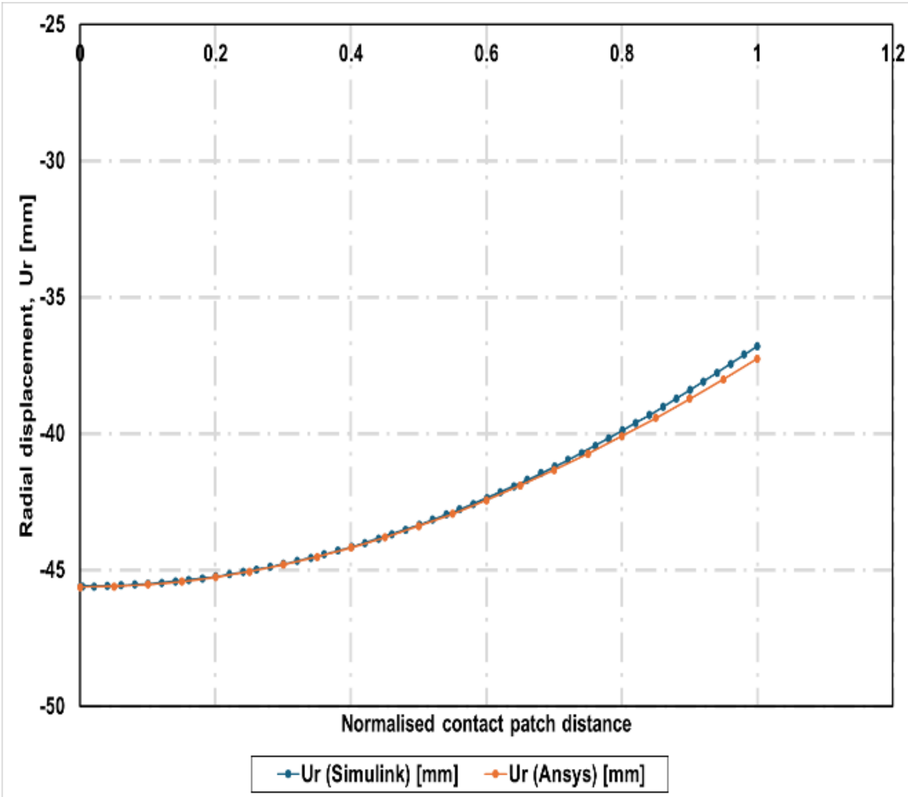

Figure 3-3 Validation plot (deformation)

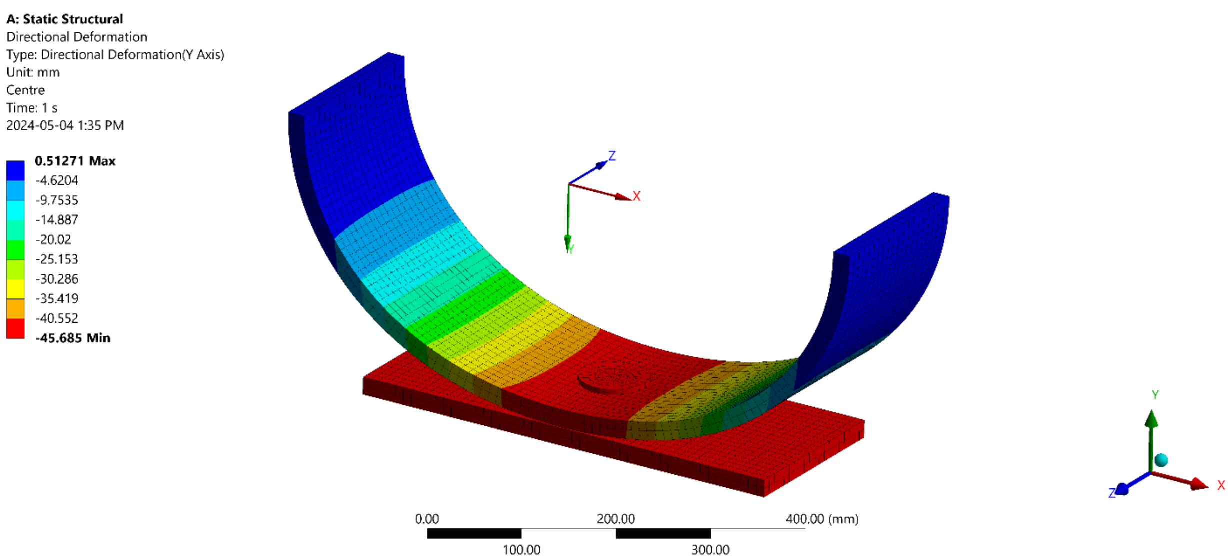

Figure 3-4 Radial deformation plot of the shear band

3.5 Summary

This chapter emphasizes the role of the shear band as a critical load-bearing component in the MPW design, tasked with ensuring uniform wheel deformation and stability. Using Timoshenko beam theory, the shear band is modeled to account for axial, bending, and shear deformations under various loads. This comprehensive modeling approach captures the complex mechanical behavior of the band, considering its composite structure of a low-shear modulus core sandwiched between inextensible membranes. Governing equations are derived for radial and circumferential displacements and cross-sectional rotation, which are solved to predict the deformation patterns in the contact patch. These analytical predictions are validated through finite element analysis (FEA), showing excellent agreement and confirming the accuracy of the theoretical model. The analysis reveals the importance of optimizing shear band material properties, thickness, and stiffness for reducing deformation and improving the wheel's load-carrying performance. The findings underscore the shear band's significance in enhancing the overall mechanical efficiency of the MPW, offering key insights into its integration within the MPW design.

Chapter 4. Finite Element Analysis of MPW

4.1 Introduction

The chapter concentrates on the computational analysis of the mechano-pneumatic wheel setup formulated in chapter 2. The analysis is particularly challenging due to the integrated structure of the shear band which acts as a support for the airbags and the airbag itself since it consists of air as a pneumatic component. Due to the following complications, a simplification of the analysis model is adapted to showcase the advantages of building an integrated sandwich shear band structure along with the pneumatic counterparts on the contact patch deformation.

4.2 FEA of the MPW with Only Air Bags as the Load Carrying Element

The section explores the advantages of addition of airbags through finite element analysis model. To study the effect of airbag entire setup is modelled in a 3D environment which is later subjected to the boundary conditions. The adapted simplified geometry of the airbag consideration is depicted in Figure 4-1. The geometrical modeling of the entire assembly is done in the CATIA V5 environment. One of the biggest simplifications adapted is the consideration of the airbag rubber pad which are in direct contact with the airbags and the Tread. It is assumed that the entire pressure loads from the airbag act on these pads. The Tread is a supporting interface structure between the rubber pads and the ground. The ground is assumed to the rigid in nature, in the current study, the ground is made of concrete, and bending is considered minimal.

Table 4-1 Material consideration in the assembly

Membrane	**Material**
Ground	Concrete
Tread	Rubber
Air bag rubber pad	Rubber

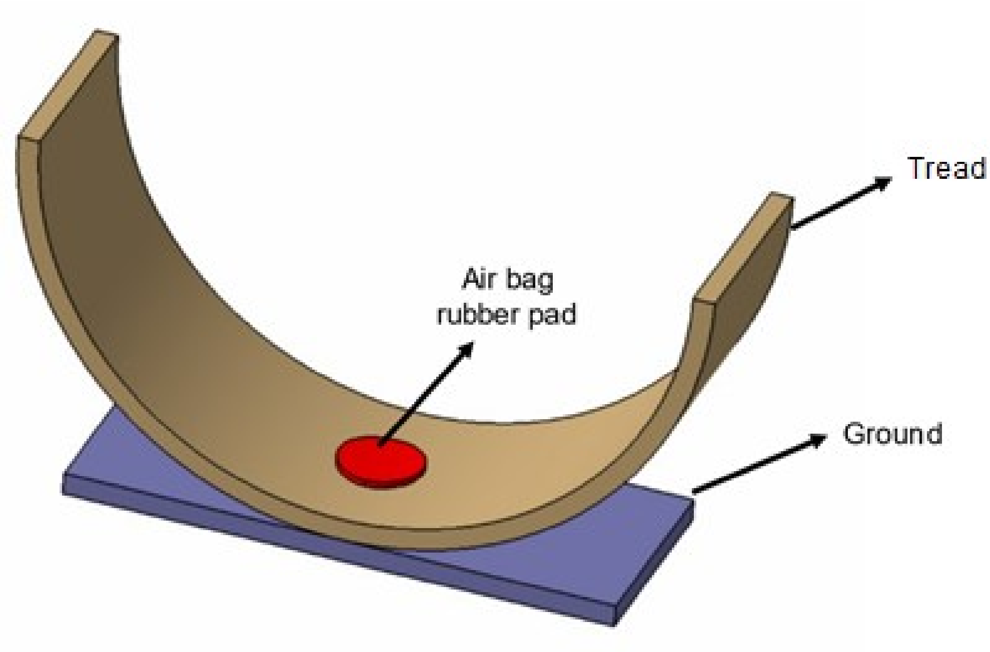

Figure 4-1 Simplified airbag representation for analysis.

4.2.1 Results

The simplified Finite Element Analysis on the 3D setup explained in the previous section is conducted using Ansys software. To study the overall deformation because of airbag, the type of analysis considered is the static structural analysis. The pressure variations and the equilibrium conditions of the airbags are discussed in chapter 0. The static analysis considerations consist of surface-to-surface contacts with finite sliding tracking approach. The sliding ensures the contact between the Tread and the ground remains free. The following contact properties are applied during the analysis.

- Frictionless bond between the Tread and the ground.
- Bonded contact between the airbag rubber pad and the Tread.
- Frictionless contact at edges of the tire.

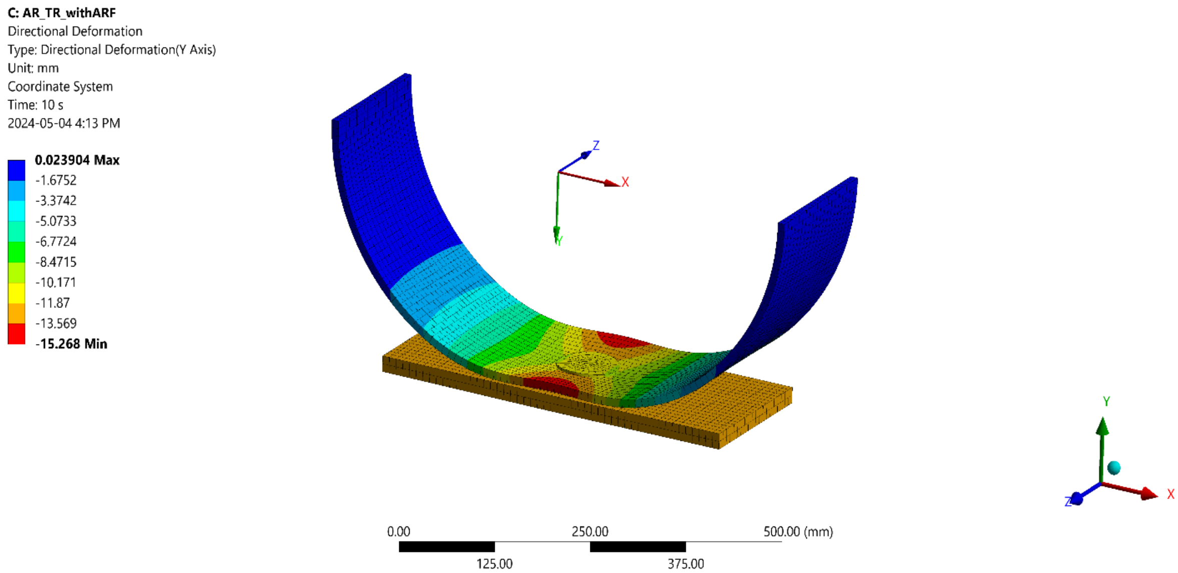

Figure 4-2 Deformation with Tread and airbag effect.

Apart from the contact regions, the edges of the tire are constrained to move only in the horizontal direction. Overall force experienced by the wheel is applied to the ground as a pressure force which will eventually be experienced by the Tread and airbag through contact constraints. Figure 4-2 shows the static structural analysis result of the airbag effect on the tire. The maximum deflection, occurs at the centre of the wheel about 15 mm. The negative deflection is due to the consideration of the coordinate system at the centre of the wheel and the deflection is in the negative y direction.

Figure 4-3 shows the contact patch deformation of the Tread subjected to pressure force from the airbag and the normal force from the ground. The maximum deflection occurs at the centre at about 15 mm and the other end of the contact patch has a deflection about 8mm when the equilibrium is attained. Compared to the shear band validation case discussed in chapter 2.11, the deflection using the shear band structure alone is 45 mm, while the airbag reduced the deflection of the wheel by 30 mm. Hence, in a mechano-pneumatic wheel setup airbag can be considered as the biggest contributor towards the setup.

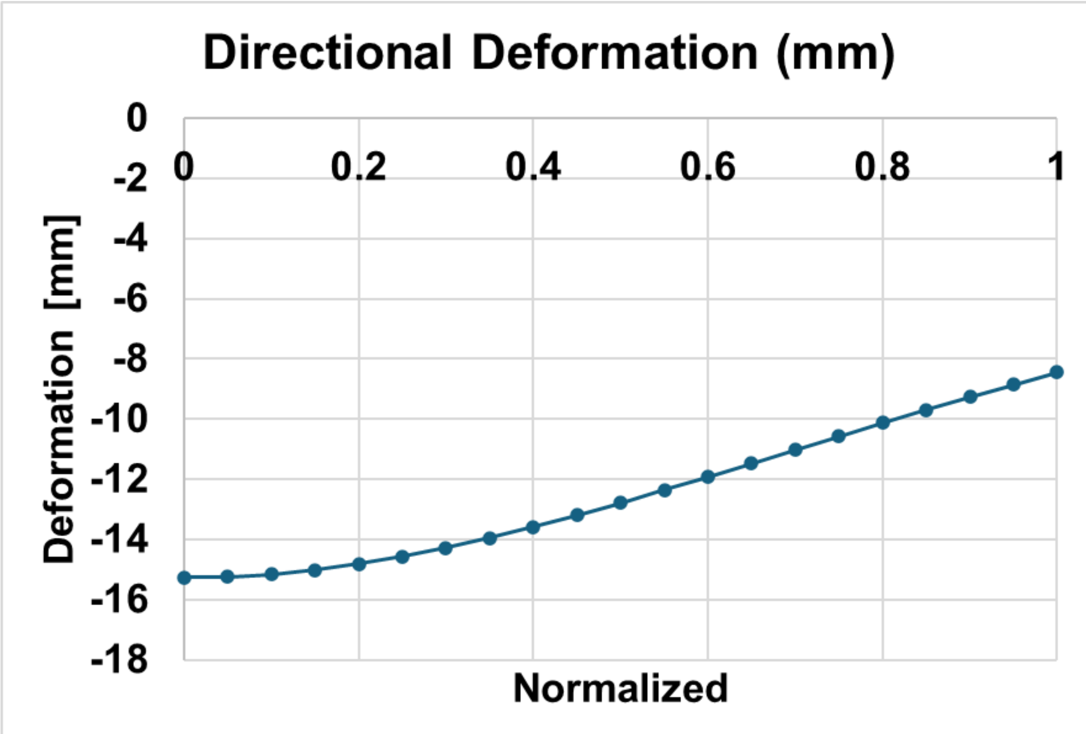

Figure 4-3 Deformation with only tread and airbag effect.

4.3 FEA of the MPW: with Air Bags and Sandwich Shear Band

The section explains the formulation of a sandwich shear band to enhance the performance of Mechano-Pneumatic Wheel setup. The sandwich consists of multi layered advanced material arrangement to improve the stress distribution and flexibility of the tire. Figure 4-4 shows the integrated model of the sandwich shear beam and the airbag adapted in the current Mechano-Pneumatic Wheel setup. The sandwich in the current setup consists of three main layers. The shear beam in the sandwich is the core layer. The core layer provides highest flexibility to the wheel evenly distributing the shear stresses. Since the core layer consist of flexible membrane, this must be reinforced with high strength material to improve the overall stiffness of the tire. The inner membrane and outer membrane are considered as the intermediate layers in the setup. These layers provide strength and stiffness to the shear band by resisting deformation and helps maintain structural integrity under heavier loads. To enhance the durability of the tire, the outer membrane is covered with the durable abrasion resistant material called Tread. This layer can be consisted as outer layer of the wheel setup. The Tread protects the inner layers from wear and damages improving overall stiffness of the band.

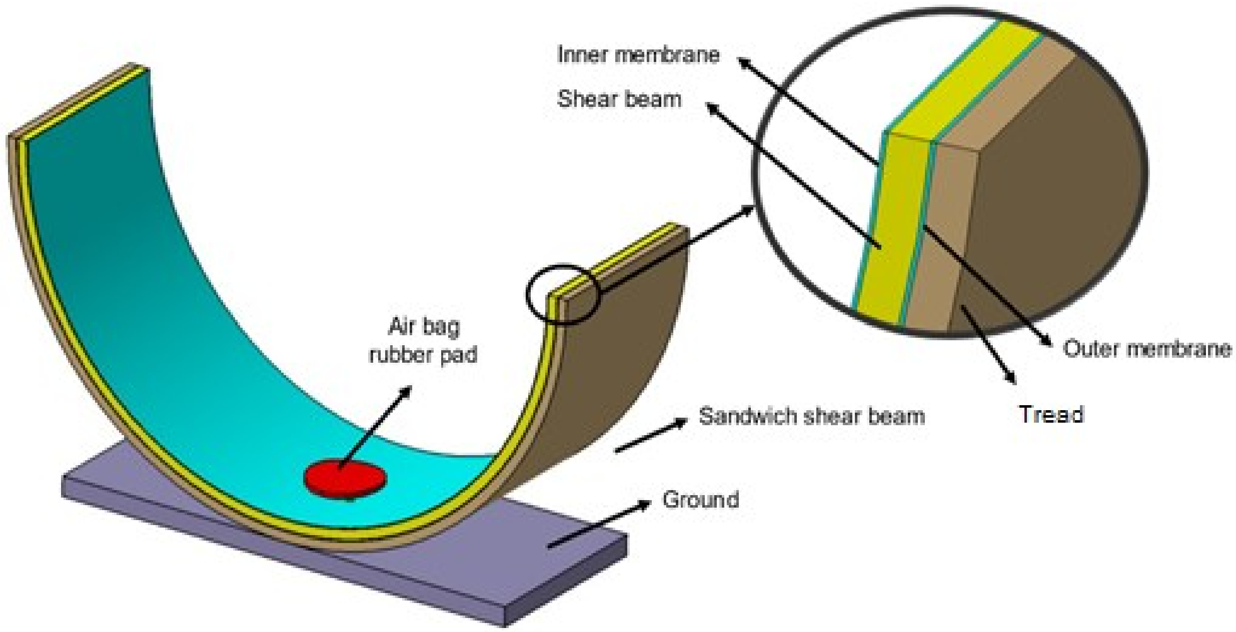

Figure 4-4 Mechano-Pneumatic Wheel sandwich model.

Table 4-2 shows the materials applied to different layers of integrated Mechano-Pneumatic Wheel setup. The shear beam is made with rubber. The outer and inner membrane is applied with high strength stainless steel. The tread is made with rubber.

Table 4-2 Materials used for the model of the sandwich Mechano-Pneumatic Wheel

Membrane	Material
Ground	**Concrete**
Outer Membrane	**Steel**
Tread	**Rubber**
Shear beam	**Rubber**
Inner membrane	**Steel**

4.3.1 Mesh and Boundary Conditions.

The integrated sandwich geometry is required to be meshed to conduct finite element analysis. The tetrahedral and hexahedral elements are the two common type of element choices for the analysis. Tetrahedral elements have the capability to analyse most complex type of geometry, however, requires more elements. Hexahedral elements require fewer elements compared to tetrahedral elements and has better accuracy when the number of elements are kept same. Figure 4-5 shows the mesh generated for the integrated sandwich structure. For the current analysis, hexahedral elements are chosen since the entire geometry is less complex due to the simplification.

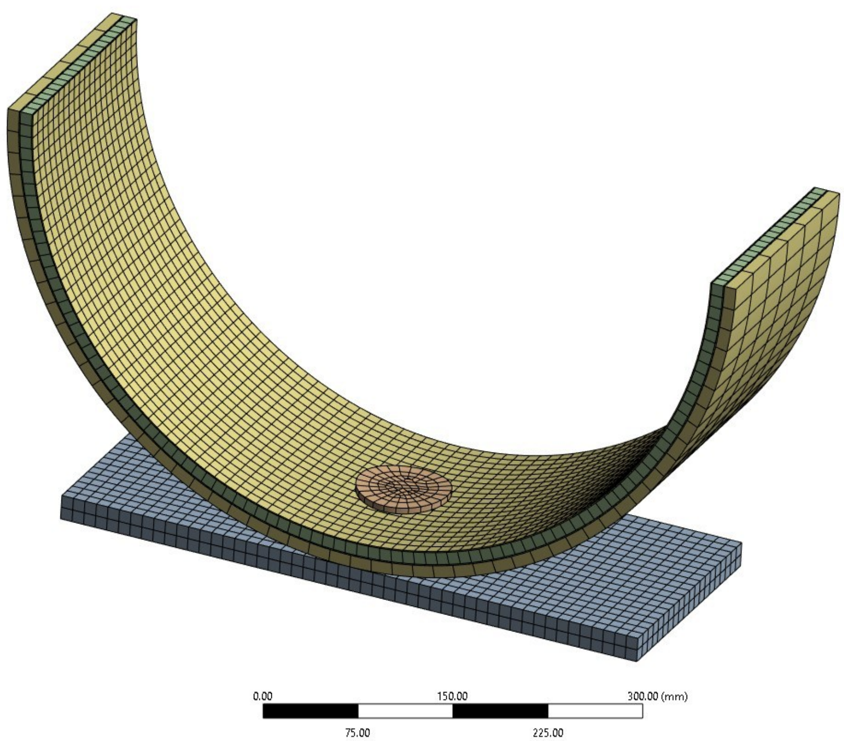

Figure 4-5 Meshed sandwich Mechano-Pneumatic Wheel model

Table 4-3 shows the boundary conditions applied to the current case study. The entire sandwich is considered as a single integrated tire component. Due to this component such as Tread, outer membrane, shear beam, inner membrane are bonded to each other. As mentioned in the previous subsection, contact between Tread and ground is considered as frictionless. The two edge of the tire is having frictionless contact to have free movement in the x direction. However, the displacement is constraint in the y and z direction. The external force on tire is applied via the ground in the -y direction. The overall contribution of the airbags is applied on the airbag rubber pads as a pressure gradient.

Table 4-3 Boundary conditions of the sandwich Mechano-Pneumatic Wheel model

Region	Contact type
Ground & Tread	Frictionless
Tread & Outer membrane	Bonded
Outer membrane & Shear beam	Bonded
Shear beam & Inner membrane	Bonded
Inner beam & Airbag rubber pad	Bonded
Edge Boundary conditions	
Region	**Edge condition**
Tread edges	Frictionless
Outer membrane edges	Frictionless
Inner membrane edges	Frictionless
Shearbeam edges	Frictionless
Reaction Force	
Region	**Value**
Airbag Pressure (Initial)	0.25 MPa
Force Ground	3000 N

4.3.2 Results

The integrated Mechano-Pneumatic Wheel sandwich static structural analysis is done using Ansys 3D FEM software to showcase the advantages. Figure 4-6 shows the results drawn on the overall deformation of the simplified geometry explained in the previous section. The maximum deformation of the integrated setup is about 12 mm. Compared to the study conducted in the previous section where the airbag setup is analysed, the current setup enjoys the advantage of reducing the overall deformation about 3 mm. It is to be noted that the stainless-steel layering in the sandwich enables the tire for additional wear and tear which cannot be fulfilled by the Tread and airbag only setup.

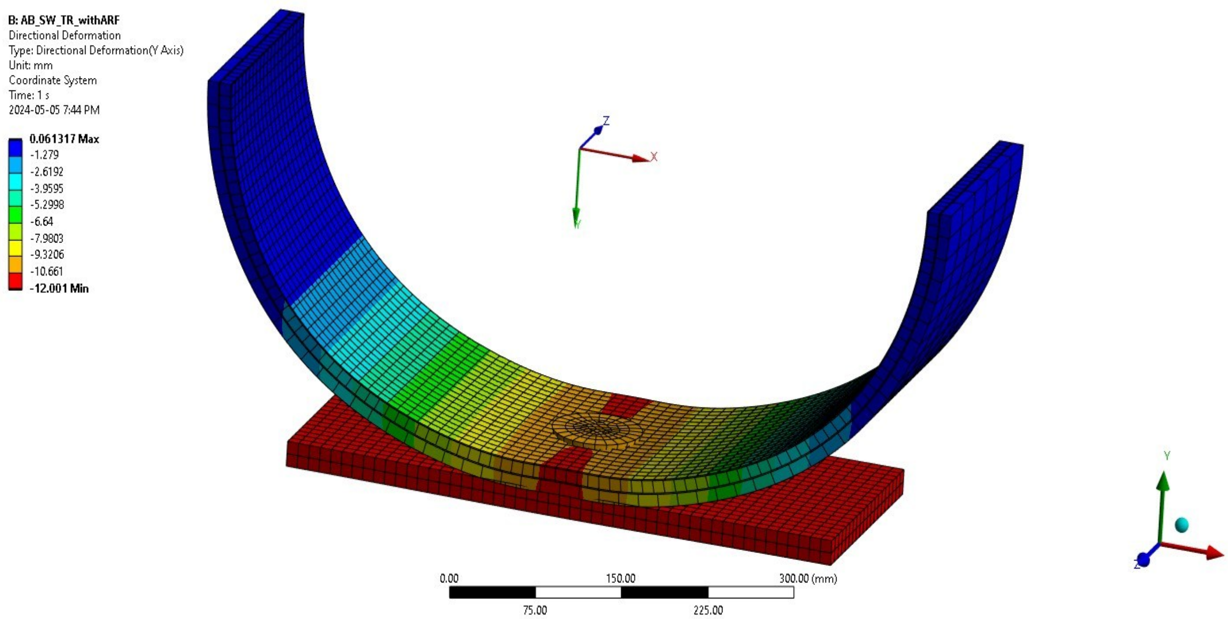

Figure 4-6 Deformation results of FEM vs MATLAB

Figure 4-7 shows the comparison of deformation plot of the contact patch region of the integrated Mechano-Pneumatic Wheel model and the shear band only setup which was validated in the previous chapter. Compared to the shear band only setup adapting an integrated Mechano-Pneumatic Wheel reduces the overall deformation at about 35 mm. This is due to the load carrying capacity offered by the airbag in combination with the sandwich structure.

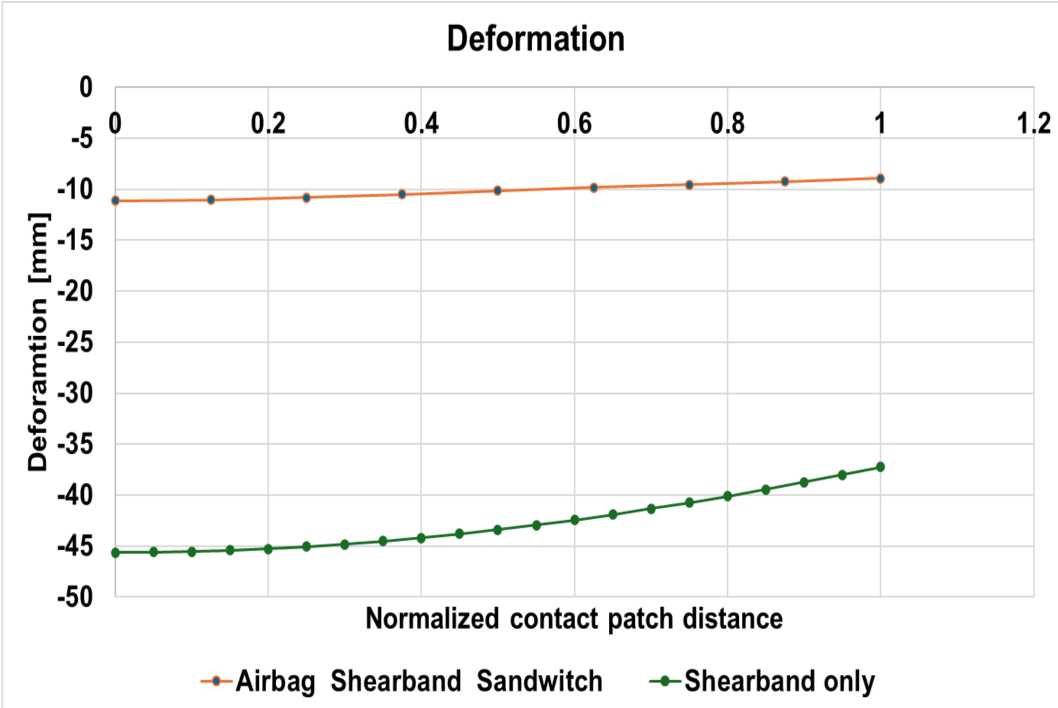

Figure 4-7 Comparison of deformation plots of two types of shear band models

4.4 Summary

This chapter presents a detailed finite element analysis (FEA) of the Mechano-Pneumatic Wheel to validate its design concepts and evaluate its structural performance. Two configurations are analyzed: one featuring only air springs as the load-carrying component, and another integrating both air springs and a composite shear band. The simulations assess various performance metrics, including radial deformation, load distribution, and equivalent vertical stiffness. Mesh refinement, boundary conditions, and material properties are meticulously defined to ensure simulation accuracy. Results indicate that the inclusion of the shear band significantly reduces radial deformation and enhances uniform load sharing across the contact patch. Comparisons between the FEA results and analytical models reveal strong consistency, affirming the theoretical predictions. This chapter highlights the FEA's critical role in identifying the MPW's mechanical behaviors under operational loads and illustrates how simulation tools can bridge theoretical design and practical implementation. The analysis underscores the MPW's potential to achieve superior performance characteristics while maintaining its innovative hybrid design.

Chapter 5. Conclusion

5.1 Major Contributions

This thesis makes significant contribution to the field of automotive wheel design by introducing the concept of Mechano-Pneumatic Wheel (MPW), that combines features of pneumatic as well as non-pneumatic wheels. The research presents a novel parallel-coupled air spring configuration, which effectively distributes the normal load and minimizes pressure fluctuations at the wheel-ground interface, while addressing common limitations of traditional pneumatic tires. The integration of a composite shear band further enhances the MPW's performance by reducing deformation at the contact patch by 3 mm. Comprehensive analytical and finite element models provide detailed insights into the wheel's mechanical behavior, especially the shear band, which was validated through simulations. By optimizing design parameters through parametric studies and advanced genetic algorithm techniques, the study achieves an ideal balance of stiffness and deformation, meeting targeted performance objectives. The MPW demonstrates potential applications across automotive, aerospace, and off-road sectors, offering a sustainable, low-maintenance alternative to existing tire designs. This work bridges critical gaps in tire technology and paves the way for future advancements in hybrid, more reliable and sustainable wheel systems.

5.2 Major Conclusions

The development of a mechano-pneumatic wheel design is a significant step in the field of automotive industry. In this context, this thesis has explored theoretical and finite element solutions, practical applications and validations of novel mechano-pneumatic wheel concept highlighting potential benefits and challenges in implementing the concept.

- It is shown that the MPW could be easily tuned to achieve the vertical stiffness of a pneumatic tire. Increasing the number of spokes permit more uniform force distribution at the contact patch. Parallel connectivity of spokes also permits greater load distribution among all the spokes.

- The effective stiffness of an MPW could be conveniently adjusted by varying the reservoir volume.

The thesis extensively reviewed multiple configurations such as pneumatic tire, non pneumatic wheel configuration such as a honeycomb wheel structure and hybrid configurations. Pneumatic tires are susceptible to puncture and blowouts, which can lead up to potential safety hazards. Moreover, pneumatic tires have limited durability and shorter lifespan. The reported non-pneumatic wheel configurations generally exhibit high vertical and lateral stiffness and there by relatively poor ride comfort due to increased vibration and shock directly to the vehicle. Moreover, they lack the ability to dynamically adjust to different load and terrain conditions due to the missing pneumatic counterpart. Given the disadvantages inherent in both pneumatic and non-pneumatic configurations, this thesis highlights the need for a hybrid configuration that combines the benefits of both pneumatic and non pneumatic configuration.

The thesis reviews three types of airbag configurations in a mechano-pneumatic wheel setup, namely, uncoupled, series coupled, and parallel coupled configuration. Highlighting the advantages of parallel coupled configuration such as reduced stresses on individual airbags, reduction of premature failure, balanced and more uniform load distribution capability and simplified design, the configuration is picked for further research. The analytical model is used to analyse the load carrying capacity of the airbag of the mechano-pneumatic configuration. Detailed analysis is done to investigate the pressure variations inside the air spring during operation. It is found from the quasi-static analysis that the airbag the pressure fluctuates between initial charge pressure of 250 MPa and peak pressure of 450 MPa.

The shear beam in a Mechano-Pneumatic Wheel configuration is considered in the current model to provide overall support and added effectiveness to the airbag. To showcase the effectiveness, an analytical model is considered, considering the shear beam as a Timoshenko beam structure. The current problem with added shear band is solved as a ring between two rigid bodies. The model validity of the shear band is examined by comparing the results of the analytical model with those of the FEM results. It is found that, considering shear band in the mechano-pneumatic configuration is beneficial in improving the overall stiffness of the wheel. However, a sandwich layer is studied to further improve the effectiveness of the wheel.

The sandwich layer configuration is proposed to improve the structural integrity of the Mechano-Pneumatic Wheel. The sandwich layer consists of layers enveloping a polyurethane compound shear band, lined up comprising with thin structural steel. The steel improves the overall strength of the material while shear band provides essential flexibility. The entire sandwich is covered with tread which is a rubber material to improve the wear and tear effectiveness. The overall analysis shows that the proposed sandwich material improves the effectiveness of the structure by reducing the overall deformation of the wheel. Overall, the integrated sandwich with the airbag is a promising configuration which can be effective for a wide range of applications, while there are still limitations with the configuration that need to be addressed through further systematic efforts.

5.3 Recommendations for Future Work

Although the Mechano-Pneumatic Wheel concept studied in the current thesis highlights the potential benefits for automotive, heavy machinery industry applications, several challenges and areas for the future research are identified and summarized below.

- The current thesis solves the problem as a static structural problem. Although, this gives a better understanding of the deformation when the convergence is achieved, dynamic analysis along with the operating conditions are required for its implementations in the automotive systems.
- Due to the analysis complexity, the current thesis simplified the airbag contribution considering the pressure acting on the airbag rubber pad, however, full scale Fluid Structural Interaction (FSI) model integrating the airbag and the shear band may be considered for more reliable analysis and performance predictions.
- The current thesis develops the methodology to analyse novel Mechano-Pneumatic Wheel concept. However, maintenance methodology or failure scenarios is yet to be considered within the model.
- Several studies have pointed out the benefits of the honeycomb wheel structures. The existing airbag integration must be studied hand in hand with honeycomb to study its relative performance. A honeycomb as a shear band structure may be considered instead of the sandwich structure to further enhance the reliability of the design.

References

[1] Gent, A. N., and Walter, J. D., "US Department of Transportation; The Pneumatic Tire," National Highway Traffic Safety Administration, 2006.

[2] Rhyne, T. B., and Cron, S. M., "Development of a Non-Pneumatic Wheel," *Tire Science and Technology*, Vol. 34, No. 3, 2006, pp. 150–169. https://doi.org/10.2346/1.2345642

[3] Darrow, B., "Pneumatic Tires - Old and New," *SAE Transactions*, Vol. 27, 1932, pp. 438–444.

[4] Tarasov, V. N., and Boyarkina, I. V, "Method of Sections in Analytical Calculations of Pneumatic Tires," *Journal of Physics: Conference Series*, Vol. 944, 2018, p. 012116. https://doi.org/10.1088/1742-6596/944/1/012116

[5] Freitag, D. R., "A Dimensional Analysis of the Performance of Pneumatic Tires on Soft Soils," Auburn University, Auburn, 1965.

[6] Popescu, S., Ciuperca, R., Nastasoiu, M., and Loghin, F., "Development and Experimental Research of the Central Pressure Control System for Agricultural Tractor Tyres," *International Automotive Congress, CONAT*, 2010.

[7] Edeskär, T., "Technical and Environmental Properties of Tyre Shreds Focusing on Ground Engineering Applications," *Luleå University of Technology, Luleå*, 2004.

[8] Roth, V., Moore, B. E., and Turner, J. L., "Geometric and Normal Contact Stress Analysis of a Rolling Tire Footprint," *SAE Transactions*, Vol. 115, 2006, pp. 1423–1435.

[9] Kenarsari, A. E., Vitton, S. J., and Beard, J. E., “Creating 3D Models of Tractor Tire Footprints Using Close-Range Digital Photogrammetry,” *Journal of Terramechanics*, Vol. 74, 2017, pp. 1–11. https://doi.org/10.1016/j.jterra.2017.06.001

[10] Melzi, S., Negrini, S., and Sabbioni, E., “Numerical Analysis of the Effect of Tire Characteristics, Soil Response and Suspensions Tuning on the Comfort of an Agricultural Vehicle,” *Journal of Terramechanics*, Vol. 55, 2014, pp. 17–27. https://doi.org/10.1016/j.jterra.2014.05.001

[11] Wang, F., Chen, H., and Cao, D., “Nonlinear Coordinated Motion Control of Road Vehicles After a Tire Blowout,” *IEEE Transactions on Control Systems Technology*, Vol. 24, No. 3, 2016, pp. 956–970. https://doi.org/10.1109/TCST.2015.2472982

[12] Shen Y, Li H, and Guo J, “Investigation on Dynamic Responses of a Heavy Vehicle with Tire Blow-Out Based on Matlab/Simulink,” *Proceedings of the 14th IFToMM World Congress*, 2015, pp. 471–485. https://doi.org/https://doi.org/10.6567/IFToMM.14TH.WC.PS17.002

[13] Zhao, Y. qun, Zang, L. guo, Chen, Y. qiao, Li, B., and Wang, J., “Non-Pneumatic Mechanical Elastic Wheel Natural Dynamic Characteristics and Influencing Factors,” *Journal of Central South University*, Vol. 22, No. 5, 2015, pp. 1707–1715. https://doi.org/10.1007/s11771-015-2689-1

[14] Dolez, P. I., Nohile, C., Ha Anh, T., Vu-Khanh, T., Benoît, R., and Bellavigna-Ladoux, O., “Exploring the Chemical Aspects of Truck Tire Blowouts and Explosions,” *Safety Science*, Vol. 46, No. 9, 2008, pp. 1334–1344. https://doi.org/10.1016/j.ssci.2007.10.004

[15] Rovira, J., Domínguez-Morueco, N., Nadal, M., Schuhmacher, M., and Domingo, J. L., "Temporal Trend in the Levels of Polycyclic Aromatic Hydrocarbons Emitted in a Big Tire Landfill Fire in Spain: Risk Assessment for Human Health," *Journal of Environmental Science and Health, Part A*, Vol. 53, No. 3, 2018, pp. 222–229. https://doi.org/10.1080/10934529.2017.1387023

[16] Ju, J., Kim, D.-M., and Kim, K., "Flexible Cellular Solid Spokes of a Non-Pneumatic Tire," *Composite Structures*, Vol. 94, No. 8, 2012, pp. 2285–2295. https://doi.org/10.1016/j.compstruct.2011.12.022

[17] Mozafari, A., Farshchi Tabrizi, F., Farsi, M., and Seyed Mousavi, S. A. H., "Thermodynamic Modeling and Optimization of Thermolysis and Air Gasification of Waste Tire," *Journal of Analytical and Applied Pyrolysis*, Vol. 126, 2017, pp. 415–422. https://doi.org/10.1016/j.jaap.2017.04.001

[18] Amir Gasmi, "On the Modeling of Contact Problems for Curved and Straight Elastic Thin Continuums with Application to Non-Pneumatic Tires," Clemson University, 2011.

[19] Deng, Y., Wang, Z., Shen, H., Gong, J., and Xiao, Z., "A Comprehensive Review on Non-Pneumatic Tyre Research," *Materials & Design*, Vol. 227, 2023, p. 111742. https://doi.org/10.1016/j.matdes.2023.111742

[20] Yang, J., Zhou, H., Zhou, H., Zheng, Z., and Wang, G., "Comparative Study of Static and Dynamic Characteristics of Non-Pneumatic Tires with Gradient Honeycomb Structure," *Journal of the Brazilian Society of Mechanical Sciences and Engineering*, Vol. 46, No. 6, 2024, p. 366. https://doi.org/10.1007/s40430-024-04967-y

[21] Suhag, A., and Dayal, R., "Static Analysis on Custom Polyurethane Spokes of Airless Tire," *International Journal of Scientific and Research Publications*, Vol. 3, No. 11, 2013, pp. 2250–315.

[22] Bras, B., and Cobert, A., "Life-Cycle Environmental Impact of Michelin Tweel ® Tire for Passenger Vehicles," *SAE International Journal of Passenger Cars - Mechanical Systems*, Vol. 4, No. 1, 2011, pp. 2011-01–0093. https://doi.org/10.4271/2011-01-0093

[23] Ju, J., Veeramurthy, M., Summers, J. D., and Thompson, L., "Rolling Resistance of a Nonpneumatic Tire Having a Porous Elastomer Composite Shear Band," *Tire Science and Technology*, Vol. 41, No. 3, 2013, pp. 154–173. https://doi.org/10.2346/tire.13.410303

[24] Jin, X., Hou, C., Fan, X., Sun, Y., Lv, J., and Lu, C., "Investigation on the Static and Dynamic Behaviors of Non-Pneumatic Tires with Honeycomb Spokes," *Composite Structures*, Vol. 187, 2018, pp. 27–35. https://doi.org/10.1016/j.compstruct.2017.12.044

[25] Kim, K., Ju, J., and Kim, D. M., "Static Contact Behaviors of a Non-Pneumatic Tire with Hexagonal Lattice Spokes," *SAE International Journal of Passenger Cars - Mechanical Systems*, Vol. 6, No. 3, 2013, pp. 2013-01–9117. https://doi.org/10.4271/2013-01-9117

[26] Kim, K., Heo, H., Uddin, M. S., Ju, J., and Kim, D.-M., "Optimization of Nonpneumatic Tire with Hexagonal Lattice Spokes for Reducing Rolling Resistance," *SAE Technical Paper*, Vols. 2015-01–1515, 2015. https://doi.org/10.4271/2015-01-1515

[27] Sardinha, M., Fátima Vaz, M., Ramos, T. R., and Reis, L., "Design, Properties, and Applications of Non-Pneumatic Tires: A Review," *Proceedings of the Institution of*

Mechanical Engineers, Part L: Journal of Materials: Design and Applications, Vol. 237, No. 11, 2023, pp. 2277–2297. https://doi.org/10.1177/14644207231177302

[28] Sidhu, C. S., and El-Sayegh, Z., "Non-Pneumatic Tire Design and Modeling: An Overview of Research," *Journal of Applied Mathematics and Physics*, Vol. 11, No. 11, 2023, pp. 3529–3564. https://doi.org/10.4236/jamp.2023.1111224

[29] Michelin, "Tweel ®: Airless Technology." https://business.michelin.ca/en/tires/tweel

[30] Manga, K. K., "Computational Method for Solving Spoke Dynamics on High-Speed Rolling Tweel™," Clemson University, 2008.

[31] Ma, J., Kolla, A., Summers, J. D., Joseph, P. F., Blouin, V. Y., and Biggers, S., "Numerical Simulation of New Generation Non-Pneumatic Tire (TWEEL™) and Sand," 2009. https://doi.org/10.1115/DETC2009-87263

[32] Aboul-Yazid, A. M., Emam, M. A. A., Shaaban, S., and El-Nashar, M. A., "Effect of Spokes Structures on Characteristics Performance of Non-Pneumatic Tires," *International Journal of Automotive and Mechanical Engineering*, Vol. 11, 2015, pp. 2212–2223. https://doi.org/10.15282/ijame.11.2015.4.0185

[33] Veeramurthy, M., Ju, J., Thompson, L. L., and Summers, J. D., "Optimisation of Geometry and Material Properties of a Non-Pneumatic Tyre for Reducing Rolling Resistance," *International Journal of Vehicle Design*, Vol. 66, No. 2, 2014, p. 193. https://doi.org/10.1504/IJVD.2014.064567

[34] Veeramurthy, M., Ju, J., Thompson, L. L., and Summers, J. D., "Optimization of a Non-Pneumatic Tire for Reduced Rolling Resistance," *International Design Engineering*

Technical Conferences and Computers and Information in Engineering Conference, Vol. 54853, 2011, pp. 861–868. https://doi.org/10.1115/DETC2011-48730

[35] Rugsaj, R., and Suvanjumrat, C., "Proper Radial Spokes of Non-Pneumatic Tire for Vertical Load Supporting by Finite Element Analysis," *International Journal of Automotive Technology*, Vol. 20, No. 4, 2019, pp. 801–812. https://doi.org/10.1007/s12239-019-0075-y

[36] Polaris Industries Inc., "Polaris Introduces Military-Grade Consumer Work Vehicle." https://ir.polaris.com/news/news-details/2013/Polaris-Introduces-Military-Grade-Consumer-Work-Vehicle/default.aspx

[37] Lee, C., Ju, J., and Kim, D.-M., "The Dynamic Properties of a Non-Pneumatic Tire With Flexible Auxetic Honeycomb Spokes," *ASME International Mechanical Engineering Congress and Exposition*, Vol. 45240, 2012, pp. 605–615. https://doi.org/10.1115/IMECE2012-88199

[38] Lee, C., Ju, J., and Kim, D.-M., "Vibration Analysis of Non-Pneumatic Tires With Hexagonal Lattice Spokes," *ASME International Design Engineering Technical Conferences and Computers and Information in Engineering Conference*, Vol. 45059, 2012, pp. 483–490. https://doi.org/10.1115/DETC2012-70538

[39] Gasmi, A., Joseph, P. F., Rhyne, T. B., and Cron, S. M., "Development of a Two-Dimensional Model of a Compliant Non-Pneumatic Tire," *International Journal of Solids and Structures*, Vol. 49, No. 13, 2012, pp. 1723–1740. https://doi.org/10.1016/j.ijsolstr.2012.03.007

[40] Gasmi, A., Joseph, P. F., Rhyne, T. B., and Cron, S. M., "Closed-Form Solution of a Shear Deformable, Extensional Ring in Contact between Two Rigid Surfaces," *International Journal of Solids and Structures*, Vol. 48, No. 5, 2011, pp. 843–853. https://doi.org/10.1016/j.ijsolstr.2010.11.018

[41] Zhao, Y., Du, X., Lin, F., Wang, Q., and Fu, H., "Static Stiffness Characteristics of a New Non-Pneumatic Tire with Different Hinge Structure and Distribution," *Journal of Mechanical Science and Technology*, Vol. 32, No. 7, 2018, pp. 3057–3064. https://doi.org/10.1007/s12206-018-0608-8

[42] Zhao, Y.-Q., Xiao, Z., Lin, F., Zhu, M.-M., and Deng, Y.-J., "Influence Analysis of Machining and Installation Errors on the Radial Stiffness of a Non-Pneumatic Mechanical Elastic Wheel," *Chinese Journal of Mechanical Engineering*, Vol. 31, No. 1, 2018, p. 68. https://doi.org/10.1186/s10033-018-0273-y

[43] Du, X., Zhao, Y., Lin, F., Fu, H., and Wang, Q., "Numerical and Experimental Investigation on the Camber Performance of a Non-Pneumatic Mechanical Elastic Wheel," *Journal of the Brazilian Society of Mechanical Sciences and Engineering*, Vol. 39, No. 9, 2017, pp. 3315–3327. https://doi.org/10.1007/s40430-016-0702-8

[44] Du, X., Zhao, Y., Wang, Q., Fu, H., and Lin, F., "Grounding Characteristics of a Non-Pneumatic Mechanical Elastic Tire in a Rolling State with a Camber Angle," *Strojniški vestnik Journal of Mechanical Engineering*, Vol. 65, No. 5, 2019, pp. 287–296. https://doi.org/10.5545/sv-jme.2018.5845

[45] Du, X., Zhao, Y., Lin, F., Fu, H., and Wang, Q., "Numerical and Experimental Investigation on the Camber Performance of a Non-Pneumatic Mechanical Elastic Wheel," *Journal of the*

Brazilian Society of Mechanical Sciences and Engineering, Vol. 39, No. 9, 2017, pp. 3315–3327. https://doi.org/10.1007/s40430-016-0702-8

[46] Zheng, Z., Rakheja, S., and Sedaghati, R., "A Comparative Study of Static and Dynamic Properties of Honeycomb Non-Pneumatic Wheels and a Pneumatic Wheel," *Proceedings of the Institution of Mechanical Engineers, Part D: Journal of Automobile Engineering*, Vol. 235, No. 14, 2021, pp. 3631–3646. https://doi.org/10.1177/09544070211007977

[47] Megan Tolley, "Harvesting the Benefits of Autonomous Agricultural Machinery." https://www.powermotiontech.com/sensors-software/automation/article/21277995/hydraforce-inc-harvesting-the-benefits-of-autonomous-agricultural-machinery

[48] Resilient Technologies, "Non-Pneumatic (Airless) Tire." https://www.oemoffhighway.com/drivetrains/tracks-tires/tires-wheels/tracks-tires/product/10343599/resilient-technologies-nonpneumatic-airless-tire

[49] Hankook, "A Future That Removes Air, And Adds Innovation." https://www.hankooktire.com/global/en/tech-in-motion/a-future-that-removes-air-and-adds-innovation.html

[50] Sulthoni, "2014 Polaris Sportsman WV850 H.O.," 2014. https://www.topspeed.com/motorcycles/motorcycle-reviews/polaris/2014-polaris-sportsman-wv850-h-o/

[51] Zheng, Z., Rakheja, S., and Sedaghati, R., “Cornering Stiffness Characteristics of Honeycomb Wheels: A Parametric Analysis Using Response Surface Method,” *Composite Structures*, Vol. 288, 2022, p. 115418. https://doi.org/10.1016/j.compstruct.2022.115418

[52] Rakheja, S., Sedaghati, R., Taghavifar, H., and Zheng, Z., “Feasibility Analysis of a Design Concept of Automotive Wheel with Pneumatic Spokes,” CONCAVE Research Centre, Mechanical Industrial & Aerospace Engineering, Concordia University, 2019.

[53] Lee, S. J., “Development and Analysis of an Air Spring Model,” *International Journal of Automotive Technology*, Vol. 11, No. 4, 2010, pp. 471–479. https://doi.org/10.1007/s12239-010-0058-5

[54] Fox, M. N., Roebuck, R. L., and Cebon, D., “Modelling Rolling-Lobe Air Springs,” *International Journal of Heavy Vehicle Systems*, Vol. 14, No. 3, 2007, p. 254. https://doi.org/10.1504/IJHVS.2007.015603

[55] Jazar, R. N., “Vehicle Dynamics,” Springer International Publishing, Cham, 2017. https://doi.org/10.1007/978-3-319-53441-1

[56] Presthus, M., “Derivation of Air Spring Model Parameters for Train Simulation,” Lulea University of Technology, Lulea, Sweden, 2002.

[57] Gavriloski, V., Jovanova, J., Tasevski, G., and Djidrov, M., “Development of New Air Spring Dynamic Model,” *FME Transactions*, Vol. 42, No. 4, 2014, pp. 305–310. https://doi.org/10.5937/fmet1404305G

[58] Goodyear, “Basic Principles of Air-Springs,” 2008.

[59] Mohan, A., Johny, C. A., Tamilarasu, A., Bhasker, J. P., and Ravi, K., “Design and Analysis of Non-Pneumatic Tyre,” *IOP Conference Series: Materials Science and Engineering*, Vol. 263, 2017, p. 062061. https://doi.org/10.1088/1757-899X/263/6/062061

[60] European Tyre and Rim Technical Organisation, “ETRTO Standards Manual,” 2007.

Appendices

Appendix A

Table A-1 Tire Load Limit at Various Cold Inflation Pressures [60]

Tyre size designation					Measuring rim width code (1)	Tyre dimensions (mm)				Load capacity (kg)		Inflation pressure (kpa)	
			Load Index			Design		Maximum in					
			Std	Reinf.		Section Width	Overall Diameter	Overall Width	Overall Diameter	Std.	Reinf.	Std.	Reinf.
155/55	R	14	69	–	5.0	162	526	168	532	325	–		
165/55	R	13	70	–	5.0	170	512	177	520	335	–		
	R	14	72	–	5.0	170	538	177	546	355	–		
	R	15	75	–	5.0	170	563	177	571	387	–		
175/55	R	13	75	–	5.5	182	522	189	530	387	–		
	R	15	77	–	5.5	182	573	189	581	412	–		
	R	16	80	–	5.5	182	598	189	606	450	–		
	R	17	81	–	5.5	182	624	189	632	462	–		
185/55	R	14	80	–	6.0	194	560	202	568	450	–		
	R	15	82	86	6.0	194	585	202	593	475	530		
	R	16	83	87	6.0	194	610	202	618	487	545		
195/55	R	13	80	–	6.0	201	544	209	552	450	–		
	R	14	82	–	6.0	201	570	209	578	475	–		
	R	15	85	89	6.0	201	595	209	603	515	580		
	R	16	87	91	6.0	201	620	209	628	545	615		
205/55	R	13	85	–	6.5	214	556	223	566	515	–	250	290
	R	14	85	–	6.5	214	582	223	592	515	–		
	R	15	88	–	6.5	214	607	223	617	560	–		
	R	16	91	94	6.5	214	632	223	642	615	670		
	R	17	91	95	6.5	214	658	223	668	615	690		
	R	18	91	–	6.5	214	683	223	693	615	–		
215/55	R	15	89	–	7.0	226	617	235	627	580	–		
	R	16	93	97	7.0	226	642	235	652	650	730		
	R	17	94	98	7.0	226	668	235	678	670	750		
	R	18	95	99	7.0	226	693	235	703	690	775		
225/55	R	13	91	–	7.0	233	578	242	588	615	–		
	R	14	91	–	7.0	233	604	242	614	615	–		
	R	15	92	–	7.0	233	629	242	639	630	–		
	R	16	95	99	7.0	233	654	242	664	690	775		
	R	17	97	101	7.0	233	680	242	690	730	825		
	R	18	98	–	7.0	233	705	242	715	750	–		